HIghly advanced Probabilistic design and Enhanced Reliability methods for high-value, cost-efficient offshore WIND

Title: Development and implementation of probabilistic and uncertainty quantification methods for reliability sensitivity analysis

Deliverable no: D5.4

Delivery date: 30-09-2024

Lead beneficiary: EDF

Dissemination level: Public

This project has received funding from the European Union's Horizon 2020 Research and Innovation Program under Grant Agreement No. 101006689

Author information (alphabetical):		
Name	Organization	Email
Asger Bech Abrahamsen	DTU	asab@dtu.dk
Suguang Dou	EDF	suguang.dou@edfenergy.com
Abel Zeghidour	EDF	
Nassif Berrabah	EDF	nassif.berrabah@edfenergy.com
Clement Jacquet	EPRI	cjacquet@epri.com
Xiaodong Zhang	DTU	
Dheelibun Remigius	DTU	

Acknowledgements/Contributions::		
Name	Name	Name

Document information:					
Version	Date	Description	Prepared by	Reviewed by	Approved by
1.0	30.09.2024	Official	Authors listed above	N. Dimitrov	N. Dimitrov

Definition:

Contents

List of Figures

1 Executive Summary

This deliverable report is focused on determining the sensitivity of the SWT2.3-93 wind turbine component reliability to the influence of environmental conditions, considering the study case of the Teesside wind farm operated in the United Kingdom by EDF. The main problem in focus is predicting the reliability of the main bearing FAG 230/800 of the turbines as quantified by the L_{10} lifetime as predicted by the implementation of the ISO 281 standard ISO281 (2007) described in Hipwerwind D5.1 and D5.2 (Remigius et al., 2023; Paz et al., 2023). The aeroelastic code Hawc2 has been used to simulate the behavior of the SWT 2.3 - 93 m wind turbine in a range of wind speeds and turbulence levels as characterized by the IEC 61400-1 wind classes, with $u =$ 4-26 m/s and reference turbulence intensities $I_{ref} = 0.1 - 0.18$. The environmental conditions at each turbine in the Teesside wind farm have been quantified in terms of the Rayleigh average wind speed V_{ave} as well as the IEC turbulence intensity I_{ref}. These parameters have been used as input for the main bearing life model and a main bearing impact map of the Teesside wind farm has been obtained to quantify the difference in reliability across the wind farm. The main findings of the work is that the aeroelastic simulations indicate that the L_{10} lifetime of the main bearings of the SWT 2.3 -93 m turbine is expected to increase slightly with increasing turbulence intensity. This result is counter-intuitive but can be explained by the peak-shaped nature of the turbine thrust curve, which is causing the largest main bearing life consumption at the peak. A higher turbulence will cause the effective time at the peak to decrease as the wind speed is fluctuating more. It has been estimated that the basic L_{10y} life of the the main bearings of the Teesside wind farm are in the range of 24-29 years. When correcting for the operational condition such as the temperature and grease viscosity as described by the a_{iso} factor then the modified main bearing lifetimes are $L_{10my} \approx 210 - 290$ years when assuming the grease remains pure during the operation. It was not attempted to obtain a characterization of the cleanliness of grease of the Teesside main bearings, but the transfer of the grease cleanliness and to the estimation of the life modification factor a_{iso} is considered the major remaining uncertainty of the physics-based main bearing life method based on the ISO 281 standard and will call for further research.

2 Introduction

This document will first provide an introduction to the methodology of estimating the life of the main bearing of a wind turbine using the ISO 281 standard ISO281 (2007). Secondly, a detailed study of the impact of the environmental conditions on the SWT 2.3 MW - 93 m turbine Siemens (2009) is provided using aeroelastic simulations to investigate the observed effect that "the main bearing life is decreasing with a decreasing turbulence intensity" as found in the previous HIPERWIND work of Deliverable D5.1 (Remigius et al., 2023). This effect has been quite counter-intuitive for the researchers involved in the drive train modeling of Hiperwind project, and an explanation is provided. Thirdly, the environmental conditions for each individual SWT 2.3 - 93 m turbine in the Teesside wind farm have been quantified in terms of the mean wind speed distribution as well the turbulence intensity using SCADA data from the wind farm. Finally, the Teesside environmental conditions are fed into the main bearing life model to provide a life map of the Teesside wind farm and a failure probability. It should be noted that the application of the ISO 218 standard to assess the lifetime of main bearings in wind turbines has recently been applied by Kenworthy et. al. in the case of a 1.5 MW GE wind turbine Kenworthy et al. (2024). The Hiperwind results are discussed in relation to the findings of Kenworthy et al. and the conclusion is presenst at the end of this report.

2.1 Teesside wind farm

The Teesside wind farm is located 1.5 km off the coast of the river Tees in the northern part of the United Kingdom(UK) near the city Middlesbrough, as illustrated in Figure 2.1. The wind farm consists of 27 SWT 2.3 - 93 wind turbines mounted on monopiles at water depths ranging between 13-16 meters. The turbines are placed in 3 rows of 9 turbines each in a North-South heading. The wind farm started operation in 2014 and is operated by EDF as of today.

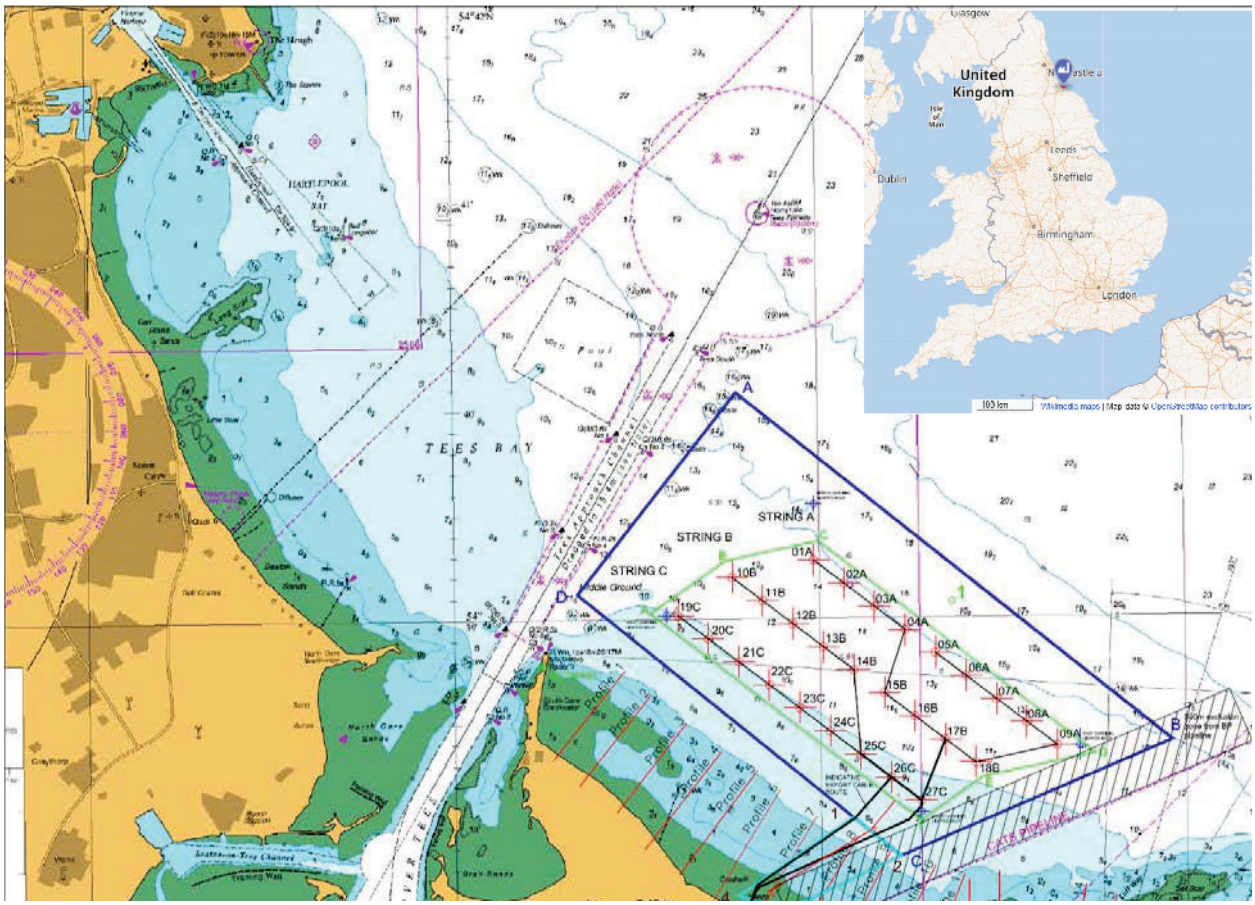

Figure 2.1: Illustration of the layout of the Teesside wind farm and the location is indicated in the inset. Reproduced from Bannister and McCall (2011)

2.2 SWT 2.3 MW - 93 m wind turbine

The Siemens Wind Turbine with the type specification SWT2.3-93 Siemens (2009) is a pitch regulated turbine with a rated power of 2.3 MW and a rotor diameter of 93 m. The drive train of the turbine consists of a 3-stage gearbox connected to a squirrel cage induction generator supported by a full power converter. This turbine model was introduced to the market in 2005 and has been installed in many offshore wind farms in Europe around 2010. In deliverable D5.1 (Remigius et al., 2023) more details on the drive train are provided and it is explained how the main bearing can be represented as a FAG 230/800 spherical double-row roller bearing as identified from spare part suppliers. Similarly, the grease used for the main bearing has been identified as Klüberplex BEM 41-301. An automatic re-greasing system will provide new grease for the main bearing from a grease cartridge mounted near the main bearing. The above properties are used as input for the main bearing life model.

3 Background

The ISO 281 standard ISO281 (2007) provides a framework of estimating the life of a population of identical bearings with similar loading and lubrication conditions. So one would expect this life distribution in a wind farm comprising many wind turbines. For a single bearing in a particular

wind turbine, it represents the probability of failure. A basic introduction to the lifetime estimation of bearings can be obtained in the book by Budynas Budynas and Nisbett (2011) and more details are provided by the technical reports TR1281 TR1281-2 (2009) and ISO 16281 as well as the technical note TPI 176 of Schaeffler Schaeffler (2013). Finally the paper by Kenworthy et. al. Kenworthy et al. (2024) is recommended introduction to the application of the ISO 281 to main bearings of wind turbines.

3.1 Basic bearing Lifetime L_{10}

The basic rating life (L_{10}) of a population of nominally identical ball or roller bearings is defined as the number of revolutions (or hours at a constant speed) that 90 percent of a population of bearings will achieve or exceed before the failure criterion is met (10% fails for a given number of revolutions), e.g., $L_{10} = 20$ means the cumulative failure probability is 10% after $20 \cdot 10^6$ revolutions, since the L_{10} lifetime has the unit of 10^6 revolutions:

$$L_{10} = \left(\frac{C}{P}\right)^b, \tag{3.1}$$

The L_{10h} lifetime with a unit of hours is defined as:

$$L_{10h} = \frac{10^6 \text{ rev}}{60 \text{ sec/min} \cdot n} \left(\frac{C}{P}\right)^b \tag{3.2}$$

and L_{10y} lifetime with a unit of years is:

$$L_{10y} = \frac{L_{10h}}{365 \text{ days/year} \cdot 24 \text{ hours/day}} \tag{3.3}$$

where C is the dynamic load capacity or basic dynamic load rating (load for the life of 1 million shaft revolutions), b is the exponent (3 for ball bearings, and $10/3$ for roller bearings), n is rotational speed (revolutions per minute (rpm)) and P is the dynamic equivalent load (in Newtons).

For radial and angular contact ball and roller bearings under constant radial and axial loads, P is given by

$$P = XF_r + YF_a, \tag{3.4}$$

where F_r and F_a are radial and axial loads, respectively. The factors X and Y are provided by the bearing manufacturer and are dictated mainly by the geometry of the bearing.

The modified rating life is given as

$$L_{nm} = a_1 a_{\text{ISO}} L_{10} \tag{3.5}$$

where a_1 is the modification factor for reliability, and a_{ISO} is the modification factor for the systems approach, including the properties and cleanliness of the grease used to lubricate the main bearing. A major challenge of quantifying the a_{ISO} factor is to account for the frictional forces of the bearing and the resulting temperature.

3.2 Life modification factor for reliability a_1

The life modification factor for reliability $a_1 = \frac{L_n}{L_{10}}$, where $L_n(T)$ is the quantile function of the distribution of time to failure $F(T_F)$, i.e., $L_n = F_{T_F}^{-1}(n/100)$. The quantile function is derived from a three-parameter Weibull distribution. A value of $L_n = T$ years corresponds to n percent probability of failure during the period T. The distribution of T_F can also be expressed in terms of L_n:

$$\begin{aligned} F(L_n) &= 1 - e^{-\left(\frac{L_n-\gamma}{\beta}\right)^{\alpha}} \\ &= \frac{n}{100} \\ &= 1 - \frac{S}{100} \end{aligned} \tag{3.6}$$

where α, β, and γ are Weibull distribution's shape, scale, and location parameters; n is the failure probability quantile and S is the survival probability quantile; and β is also referred to as characteristic life in Budynas and Nisbett (2011).

The following equation could be obtained from Eq. (3.6) and is introduced in the explanatory notes on ISO 281 in ISO/TR 1281-2:2008(E) :

$$L_n - \gamma = \beta \left(\ln \left(\frac{100}{S} \right) \right)^{1/\alpha} \tag{3.7}$$

and when $n = 10$,

$$L_{10} - \gamma = \beta \left(\ln \left(\frac{100}{90} \right) \right)^{1/\alpha}, \tag{3.8}$$

from which, β could be expressed as:

$$\beta = (L_{10} - \gamma) \,/ \left(\ln \left(\frac{100}{90} \right) \right)^{1/\alpha} \tag{3.9}$$

Introducing a factor C_γ, $\gamma = C_\gamma L_{10}$, and Eq. 3.7 could be expressed as:

$$L_n - C_\gamma L_{10} = \beta \left(\ln \left(\frac{100}{S} \right) \right)^{1/\alpha} \tag{3.10}$$

Substitute Eq. (3.9) to Eq. 3.10 and divide L_{10} at both sides, the life adjustment factor for reliability can be written as TR1281-2 (2008):

$$a_1 = \frac{L_n}{L_{10}} = (1 - C_\gamma) \left(\frac{\ln (100/S)}{\ln (100/90)} \right)^{1/\alpha} + C_\gamma \tag{3.11}$$

for S ranging from 90% to 99.95%, where $\alpha = 1.5$, and $C_\gamma = 0.05$ according to ISO 1281 TR1281-2 (2009) and also described in TPI 176 note from Schaeffler Schaeffler (2013).

From eq.(3.11) one can obtain the survival S and failure F probability in the unit of [%] as given by

$$S = 100 \cdot e^{-ln(\frac{100}{90})\left(\frac{a_1 - C_\gamma}{1 - C_\gamma}\right)^\alpha} \tag{3.12}$$

and

$$F = 100 - S = 100 \cdot \left(1 - e^{-ln(\frac{100}{90})\left(\frac{a_1 - C_\gamma}{1 - C_\gamma}\right)^\alpha}\right) \tag{3.13}$$

where $a_1 = Lnm/L_{10}$ and $\alpha = 1.5$ and $C_\gamma = 0.05$ as defined previously.

The failure rate f of a fleet of bearings can be obtained by differentiating the cumulative Weibull function

$$\begin{aligned} f(L_{nm}) &= \frac{\partial F}{\partial L_n} \\ &= 100 \cdot \left[-e^{-ln(\frac{100}{90})\left(\frac{a_1 - C_\gamma}{1 - C_\gamma}\right)^\alpha} \cdot \left(-ln(\frac{100}{90})\, \alpha \left(\left(\frac{a_1 - C_\gamma}{1 - C_\gamma}\right)^{\alpha - 1}\right) \frac{1 - C_\gamma}{L_{10}}\right] \\ &= 100 \cdot \left[ln(\frac{100}{90}) \frac{1 - C_\gamma}{L_{10}} \cdot \alpha \cdot \left(\frac{a_1 - C_\gamma}{1 - C_\gamma}\right)^{\alpha - 1} e^{-ln(\frac{100}{90})\left(\frac{a_1 - C_\gamma}{1 - C_\gamma}\right)^\alpha}\right] \end{aligned} \tag{3.14}$$

where $a_1 = L_{nm}/L_{10}$ has been used instead of writing out L_{nm}. The failure rate of the bearing as function of time can then be calculated once the L_{10} value has been determined and the parameters C_γ and α of the Weibull distribution are known.

The failure rate in terms of turbines failing per year $f_{turbine}$ can then be found by multiplying the failure rate f of eq.(3.14 with a number of turbines $N_{turbines}$ of the Teesside wind farm.

$$f_{turbines} = N_{turbines} \cdot f(L_n) \tag{3.15}$$

3.3 Life modification factor for system approach a_{iso}

The so-called modification factor for system approach a_{iso} was added to the ISO 281 standard for roller bearing ISO281 (2007) in the 2007 addition as described in the Schaeffler technical note TPI 176 Schaeffler (2013). This factor takes into account the operation condition of the bearing in terms of the grease properties as well as the operation temperature of the bearing. The modified lifetime L_{10m} of the bearing is found from the basic bearing life L_{10} by simply multiplying the a_{iso} factor onto the L_{10} lifetime as shown in eq.(3.5). Thus it simply tells if the bearing will live longer or shorter than the basic life depending on the operation state of the bearing.

Two regimes of the a_{iso} factor can be identified as

$$\begin{aligned} 1 < a_{iso} < 50 &\quad \text{Good condition with longer life} \\ 0 < a_{iso} < 1 &\quad \text{Bad conditions with shorter life} \\ a_{iso} = 1 &\quad \text{Modified life } L_{10m} \text{ equal to basic life } L_{10} \end{aligned} \tag{3.16}$$

The determination of the a_{iso} factor has been described in the Hiperwind deliverable report D5.1 Remigius et al. (2023) and D5.3 Abrahamsen et al. (2024) in terms of the input for the SWT 2.3 - 93 wind turbine and also a method for solving the equations related to the parameters of the a_{iso} factor as provided in the ISO 281 standard ISO281 (2007), the technical notes ISO/TR 1281 TR1281-2 (2009) and the technical note on roller bearing lubrication from Schaeffler Schaeffler (2013). The paper of Kenworthy et. al. is also providing an introduction to the life modification factor Kenworthy et al. (2024).

In this report, the resulting a_{iso} factor is shown based on the aeroelastic simulations of the SWT 2.3 - 93 turbines of the Teesside wind farm.

4 Methodology

4.1 Main bearing loads from aeroelastic simulations

In order to determine the main bearing loads one can perform aeroelastic simulations of a turbine model when exposed to the environmental condition of an installation site. The aeroelastic code Hawc2 Larsen and Hansen (2023) as used to perform the simulations and a SWT 2.3 - 93 turbine model was created as part of the Hiperwind project in collaboration with EDF. The Hawc2 model of the turbine is confidential and can not be shared, but the preparations of the load simulations are described in the following.

The Design Load Case DLC 1.2 of the IEC 61400-1 standard determines the fatigue loads with a normal turbulence model (NTM) when a wind turbine is under normal operation IEC61400 (2019). For the NTM, the mean of 10 minutes wind speed at hub height u is described by a Rayleigh distribution with a probability distribution function (PDF):

$$f(y) = \frac{u}{s^2} e^{-u^2/2s^2} \tag{4.1}$$

where $s = \sqrt{\frac{2}{\pi}} V_{ave}$ is the scale parameter, and V_{ave} is annual average wind speed. The shape of the PDF is fully governed by the single parameter V_{ave}. The Rayleigh distribution is a simplification of the more general Weibull wind speed distribution, where the so-called shape parameter k is equal to $k = 2$. The IEC 61400-1 standard defines a set of IEC wind classes named I, II and III related to the average wind speed of $v_{ave} = 10$, 8.5 and 7.5 m/s respectively IEC61400 (2019).

According to the IEC model, the turbulence is considered conditionally dependent on the mean wind speed, with probability distribution parameters which are linear functions of the mean wind speed. The slope of this linear relationship depends on the turbulence class, and is anchored to I_{ref}, a reference quantile value of the turbulence at mean wind speed at hub height $u = 15$m/s.

$$\sigma_1 = \mathrm{I}_{ref}(0.75u + b) \tag{4.2}$$

where u is the wind speed, I_{ref} the reference turbulence intensity and the constant $b = 5.6m/s$. Note that there is a difference between IEC 61400-1 editions 3 and 4 of the standard, where until edition 3 the turbulence σ_u should follow a lognormal distribution and I_{ref} should represent its 90% quantile at $u = 15$m/s, while from edition 4 σ_u is defined as Weibull-distributed and I_{ref} as the 70% quantile at $u = 15$m/s. σ_1 is thus referred to as *characteristic* turbulence as it does

not represent the mean, but a different quantile which is deemed more representative for load assessment.

The IEC wind classes also contain a letter A, B or C, corresponding to a reference turbulence intensity of $I_{ref} = 0.16$, 0.14 and 0.12 respectively.

Thus the wind environment that a wind turbine is exposed to, according to the Design Load Case DLC 1.2, is mainly characterized by the annual average wind speed v_{ave} of the Rayleigh or Weibull distribution, and the reference turbulence intensity I_{ref}. In the following it is described how the aeroelastic code Hawc2 was prepared to calculate 600 seconds time series response of the SWT2.3 - 93 turbine when exposed to a range of wind and turbulence conditions (encompassing the said IEC wind classes) in order to investigate the effect of the environmental conditions on the main bearing life.

The wind speed is divided into $m = 23$ bins, where the bin center ranges from 4-26 m/s with a step of 1 m/s. The corresponding σ_1 is calculated from Eq. 4.2 with I_{ref} varying from 0.10 to 0.18 with a step of 0.002, resulting in 41 values.

The representative turbulence intensity is calculated as

$$TI = \frac{\sigma_1}{u} = \frac{\mathrm{I}_{ref}(0.75u + b)}{u} \tag{4.3}$$

where the b-value is assumed constant at $b = 5.6$ m/s.

Three wind directions of an angle of 0, 10, and 350 degree with respect to the yaw angle of zero degrees, are considered at each wind speed bin in order to represent a rotor misalignment. The wind speed bins, I_{ref}, and wind directions give $23 \times 41 \times 3 = 2829$ combinations characterized by the 10 min wind speed u and the turbulence intensity TI of each simulation. Each combination is assigned 12 seeds for turbulence box generations, resulting in $N = 12 \times 2829 = 33948$ simulations in total, where a random wave seed is applied for each simulation. This represents about 236 days of turbine operation of design load case DLC 1.2. With a normal personal computer the time it takes to perform the aeroelastic simulations is about the same as the simulated time. The Sophia supercomputing cluster at DTU Wind and Energy System, was therefore used. The details of the aeroelastic simulation setup can be found in HiperWind deliverable D5.1.

4.2 Post-processing aeroelastic loads

After the Hawc2 simulations have been obtained then one will have to determine the damage accumulation or the equivalent load of the main bearing of each 600 second time simulation. In order to identify the method for this it is instructive to revisit the bearing life equation as formulated in eq. (3.5) and to write out the terms, which are time dependent.

$$L_{nm} = a_1 a_{\mathrm{ISO}}(t) L_{10}(t) = a_1 a_{\mathrm{ISO}}(t) \frac{10^6}{60 n(t)} \left(\frac{C}{P(t)} \right)^b \tag{4.4}$$

where $a_{iso}(t)$ is time dependent, because the temperature or grease cleanliness can change during a simulation time series, $n(t)$ is the rotation speed of the bearing that will change during a 600 s simulation and finally the load $P(t)$ will also change during a 600 s simulation. An infinitesimal damage contribution can now be formulated as

$$dD = \frac{(P(t))^b n(t) dt}{a_{iso}(t)} \tag{4.5}$$

where dt is an infinitesimal time increase. The damage accumulation is then obtained by integrating over time, whereby the following expression is obtained

$$D = \int dD = \int_{t=0}^{t_i} \frac{(P(t))^b n(t) dt}{a_{iso}(t)} \tag{4.6}$$

A damage equivalent load P_{eq} can be obtained by assuming the P is constant and can be moved in front of the integral.

$$\int_{t=0}^{t_i} \frac{(P(t))^b n(t) dt}{a_{iso}(t)} = P_{eq}^b \int_{t=0}^{t_i} \frac{(n(t) dt}{a_{iso}(t)} \Rightarrow P_{eq} = \left(\frac{\int_{t=0}^{t_i} \frac{(P(t))^b n(t) dt}{a_{iso}(t)}}{\int_{t=0}^{t_i} \frac{(n(t) dt}{a_{iso}(t)}} \right)^{1/b} \tag{4.7}$$

where the time t_i is the time period of a single time simulation. In case the a_{iso} factor can be considered constant over the time span of the simulation then this can be omitted. The equivalent load as given by eq. (4.7) is needed for the case of both varying loads and rotation speed of the simulated time series. This integral form of the equivalent load is found in the technical note TPI 176 of Schaeffler Schaeffler (2013).

One can reduce the equivalent load to a discrete version by representing the integrals by sums as shown below. The mean dynamic equivalent load of a 10 min time series P_k, for $k = 1, 2, ..., N$, is:

$$P_k = \sqrt[b]{\frac{\sum_{i=1}^{n_t} P_i^b l_i}{\sum_{i=1}^{n_t} l_i}} = \sqrt[b]{\frac{\sum_{i=1}^{n_t} P_i^b \omega_i t}{\sum_{i=1}^{n_t} \omega_i t}} = \sqrt[b]{\frac{\sum_{i=1}^{n_t} P_i^b \omega_i}{\sum_{i=1}^{n_t} \omega_i}}, \tag{4.8}$$

where P_i is the equivalent load (from Eq. (3.4)), and l_i is the associated number of revolutions, where ω_i is the rotational speed at each time instance, and t is the time step of the simulation, and n_t is the number of points for a 10 min simulation. The L_{10} value at each time series $L_{10,k}$ could be calculated from Eq. (3.2).

For a specific I_{ref}, at each wind bin, the mean of $L_{10,k}$ values from 36 simulations (combinations of three wind directions and 12 seeds) is obtained as $L_{10,j}$, for $j = 1, 2, ..., m$. The L_{10} aggregating all $L_{10,j}$ values from all wind bins is:

$$L_{n\eta} = \frac{1}{\sum_{j=1}^{M} \frac{f_j}{\eta L_{10,j}}}, \tag{4.9}$$

where f_j is the frequency of the jth wind speed bin obtained from the Rayleigh distribution in Eq. (4.1). $\eta = 1$ gives the basic L_{10} with a failure rate of n = 10%, $\eta = a_1$ gives the L_n with life modification factor for reliability a_1 and a failure rate of n%, $\eta = a_{\text{ISO}}$ gives the modified lifetime L_{10m} with a_{ISO} factor and a failure rate of 10%, and $\eta = a_1 \times a_{\text{ISO}}$ gives the modified life L_{nm} with both factors and a failure rate of n%. The derivation of eq.(4.9) is provided in Kenworthy et. al. Kenworthy et al. (2024) and in Budynas and Nisbett (2011).

4.3 Wind environmental characterization

In order to determine the environmental conditions at each of the wind turbines of the Teesside wind farm, an analysis of the SCADA data was performed. Each turbine is equipped with an anemometer and a wind vane mounted behind the turbine rotor in order to measure the wind speed and the wind direction. These measurements are used by the wind turbine controller to control the pitch angle of the wind turbine blades as well as the yaw angle of the turbine rotor. The wind turbine controller will also determine the 10- minute average wind speed u_{10min} as well as the standard deviation of the wind speed in the 10-minute averaging window σ_u and output this information in the SCADA data transmitted from the wind turbines. A database is collecting all the SCADA data with 10-minute time resolution and post-processing can be performed to investigate the status and behavior of the turbines. Approximately four years of processed and filtered SCADA data are available for the study.

The first variables to be determined are the parameters of the wind speed distribution at each turbine. As a simplification and in order to make a more robust fit to noisy data, we consider a Rayleigh distribution fit with one parameter (V_{ave}) rather than a 2-parameter Weibull distribution. The fitting process then amounts to computing V_{ave} at each turbine.

The other required environmental parameter, I_{ref}, can be obtained from the same observations. This can be done by directly binning the data and taking I_{ref} as the average from the bin corresponding to $u = 15$ m/s and $F(\sigma_u) = 0.9$, or by using Eq.(4.2) to make a linear fit using the entire range of available wind speed data.

5 Results

The results will be presented starting with the aeroealstic simulation of the main bearing loads and the resulting main bearing life model. Secondly, the mapping of the wind speed and turbulence intensities at the Teeesside wind farm is shown along with the fitted environmental parameters in terms of the average wind speed v_{ave} and IEC reference intensity I_{ref} of each turbine. Finally, the Teesside turbine parameters are fed into the main bearing life model to estimate the lifetime of the main bearings.

5.1 Aeroelatic simulation of environmental impact

The aeroelastic code HAWC2 Larsen and Hansen (2023) was used to perform time simulations of the loads of the SWT2.3-93 turbine and the main bearing axial and radial loads were obtained from the node representing the main bearing in the model. The details of the Hawc2 model were provided by EDF and cannot be shared due to confidentiality. An overview of the 33948 simulations will be provided in a series of contour plots showing the main bearing loads as function of the wind speed u and turbulence intensity TI, which is the input setting of each simulation. Since the turbulence intensity is described by the IEC normal turbulence model then the plot shows the trajectories of eq.(4.2).

A typical determination of the equivalent load of the main bearing is shown in Figure 5.1 and the details of applying the geometric weight factors of eq.(3.4) is illustrated in Figure 5.2.

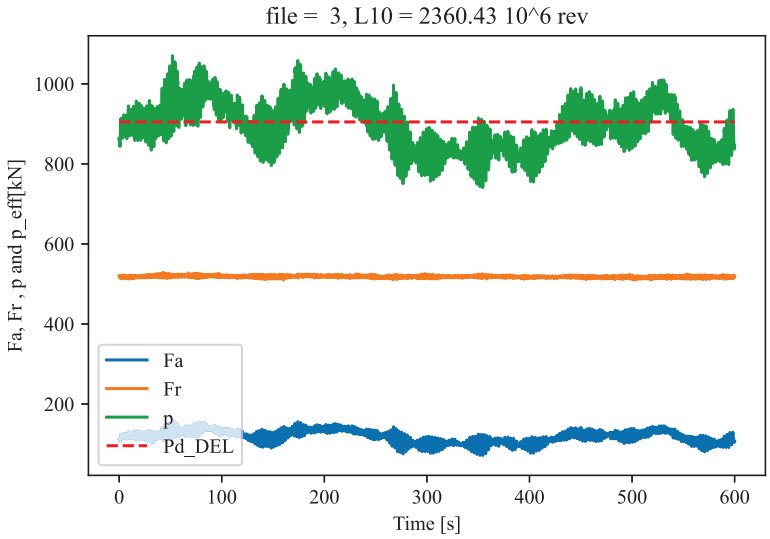

Figure 5.1: Example of the main bearing axial F_a and radial F_r loads of time series of an aeroelastic simulations with an average wind speed of $v_{ave} = 4$ m/s and a turbulence intensity of $TI = 0.215$ corresponding to an $I_{ref} = 0.1$. The resulting bearing load P given by eq. (3.4) and the equivalent load Pd DEL given by eq. (4.7) are shown at the top.

Figure 5.3 and Figure 5.4 show the variation of the axial and radial loads entering the main bearing of the large aero-elastic simulation dataset. It is seen that the axial load is peaking up at the rated wind speed as expected, since the axial load is basically given by the thrust load of the turbine. The radial loads are almost constant at around $F_r =$ 505-523 kN, which can be

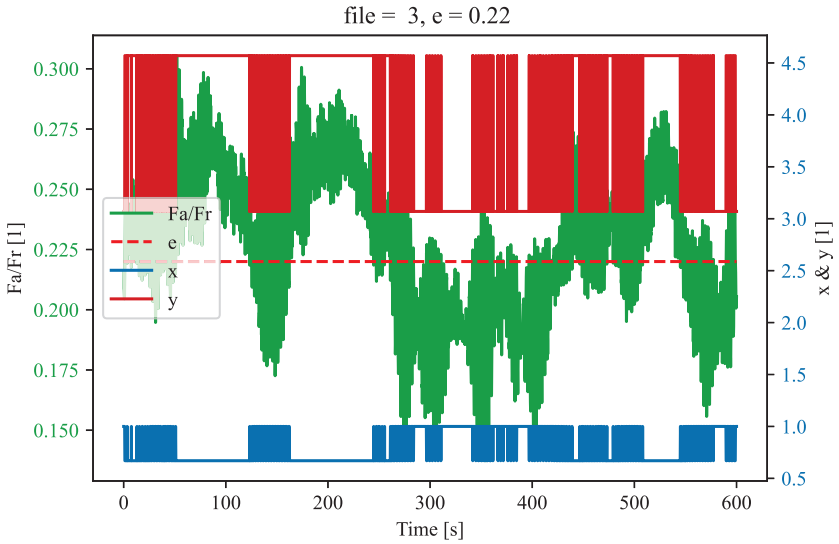

Figure 5.2: Example of determining the geometrical weight factors involved in the calculation of the main bearing effective load from the axial F_a and radial F_r loads of Figure 5.1. When the ratio between the axial and radial load is larger than the parameter e = 0.22 then different weights X and Y must be applied for the FAG 230/800 bearing. $(X, Y) = (1, 3.07)$ when $F_a/F_r < e$ and $(X, Y) = (0.67, 4.57)$ when $F_a/F_r > e$

explained as the weight of the turbine rotor resting primarily on the main bearing and, to some extent, on the gearbox front bearing. The SWT 2.3 - 93 turbine rotor weight is listed to be m_{rotor} = 60 ton in the turbine brochure Siemens (2009), and this corresponds to a gravitational load of $F_g = m_{rotor} g \approx 589\, kN$.

Figure 5.5 shows the equivalent load of the main bearing of the aeroelastic time series simulations as obtained by applying eq. (4.7) to the axial and radial loads as illustrated in Figure 5.1 and 5.2. It is observed that the equivalent loads are peaking around the rated wind speed v_{rated} of the turbine as expected from the thrust curve of the turbine. It is however very important to point to the fact that a clear decrease of the equivalent main bearing load is observed as the reference turbulence intensity is increased from $I_{ref} = 0.1$ at the bottom of the graph and above an $I_{ref} > 0.14$. The origin of this decrease will be discussed further in this report and it is related to the peak shape of the thrust curve and the implementation of the pitch controller of the turbine.

There are many additional operational parameters that were checked for the aeroelastic simulations to understand if they showed a dependence on the turbulence intensity and the following figures will provide an overview of these.

Figure 5.6 shows the thrust load of the turbine and it is observed that the levels are quite similar to the axial load shown in Figure 5.3. Secondly, the effects of a decreasing thrust for an increasing reference turbulence intensity is also observed as was the case for the main bearing axial loads. Figure 5.7 is showing the power production of the turbine as function of the wind speed and turbulence intensity. Here it is interesting to observe that the maximum power production is first obtained at higher wind speeds as the reference turbulence intensity is increased from an IEC wind class C with $I_{ref} = 0.12$ and towards a class A with $I_{ref} = 0.16$ or higher. This effect can

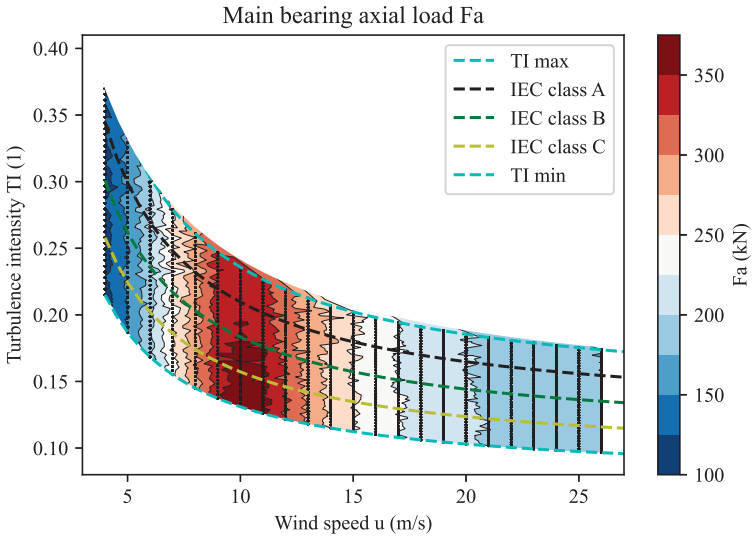

Figure 5.3: Overview of main bearing axial load F_a of the aeroelastic simulation representing u = 4-26 m/s and I_{ref} = 0.1-0.18. The IEC turbulence wind classes A, B and C with I_{ref} = 0.16, 0.14 and 0.12 are shown by dashed lines.

be explained by wind fluctuations bringing the wind speed below the rated wind speed, whereby the production decreases in that time interval.

Figure 5.8 and Figure 5.9 show that the turbine torque and pitch settings are independent of the turbulence intensity, which is also expected since the rated wind speed v_{rated} and the pitch controller settings are not based on any information about the turbulence.

This study has attempted to also include a determination of the heating of the main bearing due to the frictional forces, which are related to the bearing loads. Figure 5.10 shows the expected temperature of the main bearing, when using a very simple heat model that will balance the heat dissipation of the main bearing with the cooling path to the temperature environment of the nacelle. This model will not take into account the heat capacity of the shaft and the bearing steel, whereby it is not expected to describe the time-delay of temperature changes. It will however reflect that the average long-term temperature is primarily a function of the wind speed and then secondly to the wind speed history. The latter is hard to represent in the aeroelastic simulations and the implications of these assumption will be discussed later in this report as well in the Hiperwind deliverable report D5.3. It should be noted from Figure 5.10 that the temperature is basically a replicate of the main bearing equivalent load P_{eq} from Figure 5.5 and is peaking up at the rated wind speed v_{rated}. Secondly it should be noted that the temperature increase at rated wind speed is estimated to be about $\Delta T = 24^oC$ above the ambient temperature of the nacelle. It should be noted that this simple estimation of the main bearing temperature is more realistic than the first main bearing temperature predictions shown in the Hiperwind deliverable report D5.1, where the maximum main bearing temperature was found to be $T_{mb,max} \approx$ 67-73 ^oC. The latter was caused by an underestimation of the heat conduction of the steel structures supporting the main bearing. The thermal model is discussed further in deliverable report D5.3 Abrahamsen et al. (2024).

As part of estimating the main bearing temperature one will have to solve the equations of the

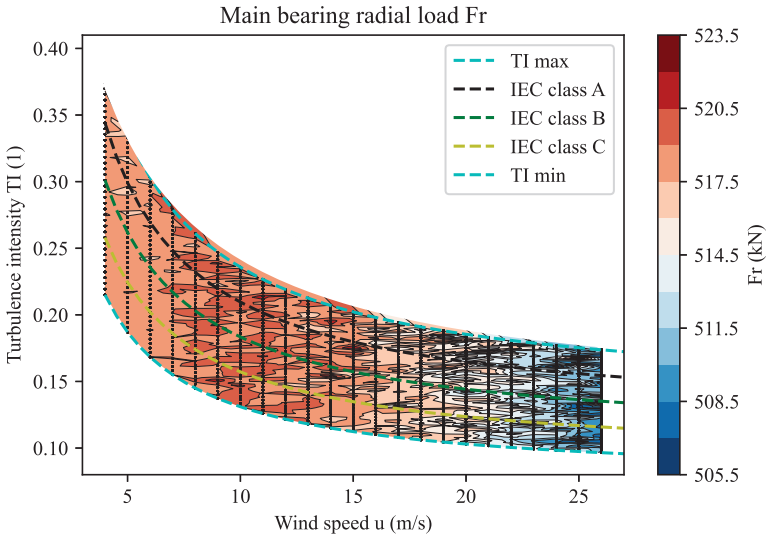

Figure 5.4: Overview of main bearing radial load F_r of the aeroelastic simulation representing u = 4-26 m/s and I_{ref} = 0.1-0.18. The IEC turbulence wind classes A, B and C with I_{ref} = 0.16, 0.14 and 0.12 are shown by dashed lines.

operating viscosity, the viscosity ratio and finally provide an estimate of the a_{iso} factor describing the modification of the bearing life due to operation conditions like the cleanliness of the grease used to lubricate the main bearing.

Figure 5.11 show how the viscosity of the Klüberplex BEM 41-301 grease of the SWT2.3 - 93 turbine FAG 230/800 main bearing is expected to change due to the main bearing temperature and operation conditions corresponding to the aeroelastic simulations in accordance to ISO 281 ISO281 (2007). The resulting viscosity ratio of the grease is shown in Figure 5.12 and finally the life modification factor due to operation a_{iso} is shown in Figure 5.13 and Figure 5.14. Here it is interesting to observe that the modified life of the main bearing will increase with the a_{sio} factor and this will be more than a factor of 10 when the wind speed is below about $u < 7\,m/s$ and above $u > 12\,m/s$. This corresponds to the operation region of low loads. It is however different for wind speeds close to the rated wind speed v_{rated} and the a_{iso} attain a minimum value of $a_{iso,min} \approx 6 - 8$ for $u = 10\,m/s$.

Finally the basic L_{10y} main bearing lifetime is shown in Figure 5.15 and it is observed that very long basic lifetimes are seen at low and high wind speeds, whereas shorter lifetimes are observed around the rated wind speed v_{rated}. Figure 5.16 shows the distribution of shorter lifetime near the rated wind speed of the turbine and also that the basic lifetime increases as the turbulence is increased.

Now the combined lifetime of the main bearing as given by eq.(4.9) has been determined by imposing the Rayleigh wind speed distribution function according to eq.(4.1) and tracing the turbulence intensities with respect to the IEC Normal turbulence Model as given by eq. (4.3). Figure 5.17 shows the resulting basic L_{10y} life of the main bearing of the SWT2.3 - 93 turbines when the environmental parameter of the input wind are changed in terms of the average wind speed v_{ave} of the Raighley distribution as well as the turbulence intensity I_{ref}. The original SWT2.3-93 turbine design IEC wind class of IIA corresponding to v_{ave} = 8.5 m/s and I_{ref} =

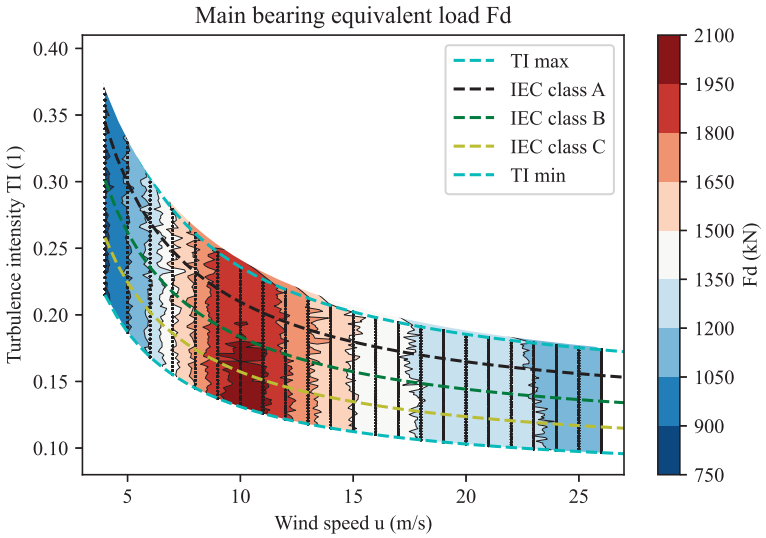

Figure 5.5: Overview of main bearing equivalent load P_{eq} of the aeroelastic simulation representing u = 4-26 m/s and I_{ref} = 0.1-0.18. The IEC turbulence wind classes A, B and C with I_{ref} = 0.16, 0.14 and 0.12 are shown by dashed lines.

0.16 is marked by a dot and the average wind speed v_{ave} = 7.1 m/s of the Teesside wind farm is marked by a dashed line Papatzimos et al. (2018). Thus it is observed that the main bearing lifetime is $L_{10y} \approx$ 23 years at the IEC design wind class IIA and that this can increase to about 27 years when positioned in the Teesside wind farm depending on the reference turbulence intensity. This basic main bearing lifetime corresponds well with the intention of having a 25-year design lifetime of an offshore wind turbine. Finally, one can determine the main bearing modified lifetime L_{10my} by including the a_{iso} factor of Figure 5.13 and Figure 5.18 shows the result. It is observed that the modified lifetime $L_{10my} \approx$ 225-300 years and thereby an order of magnitude larger than the offshore wind turbine design lifetime of 25 years. Thus one could claim that the operation of the SWT 2.3 - 93 turbine will be safe at the Teesside offshore wind farm. This is probably an effect of estimating the grease as clean as possible. Both the basic and modified main bearing life will be compared to the operation of the Teesside wind farm.

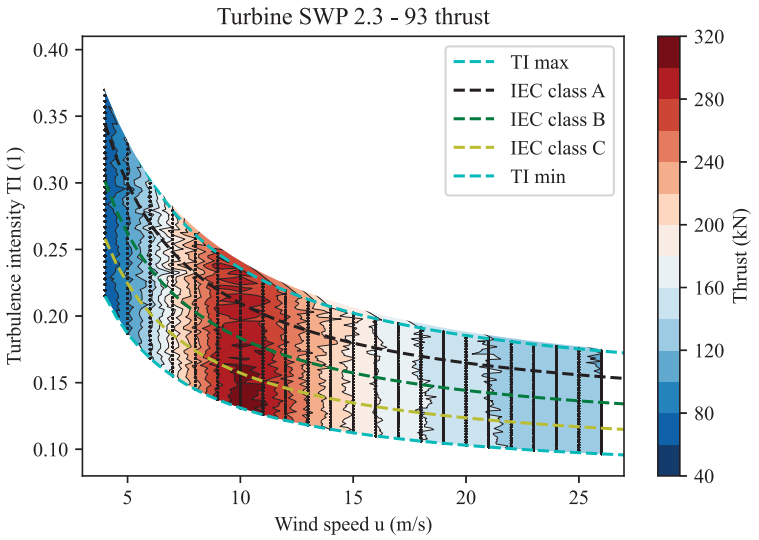

Figure 5.6: Thust load map of the aeroelastic simulations as function of wind speed u and turbulence intensity TI.

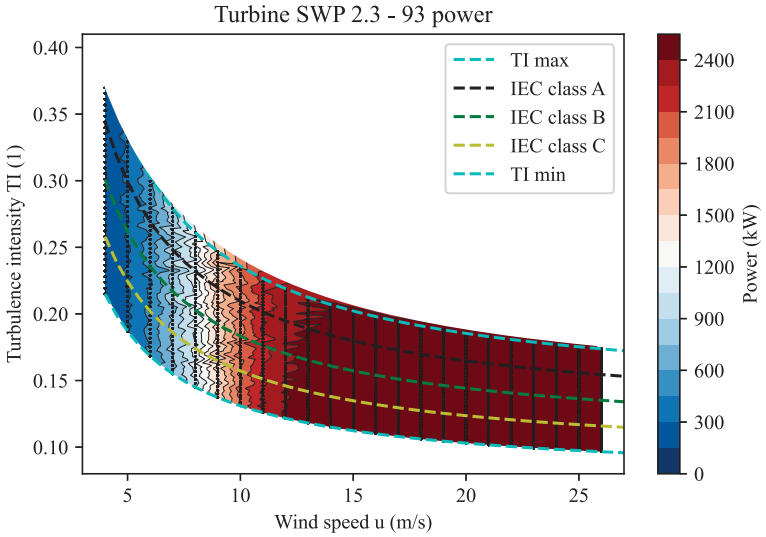

Figure 5.7: Power production map of the aeroelastic simulations as function of wind speed u and turbulence intensity TI.

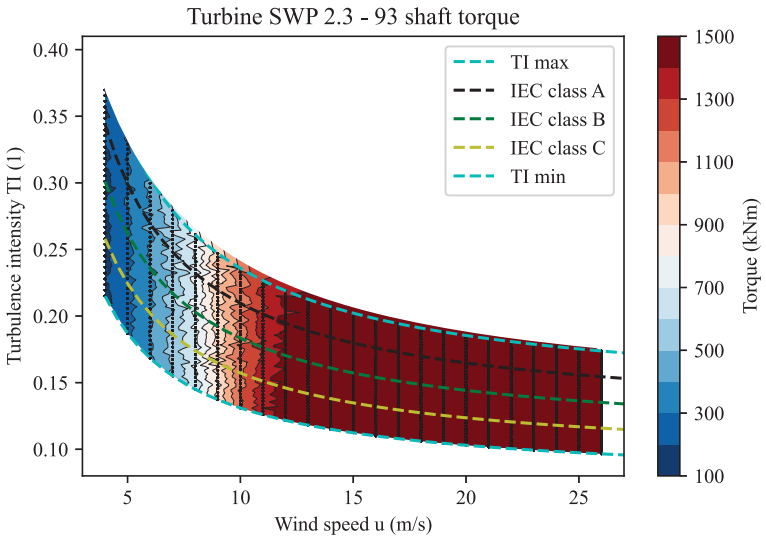

Figure 5.8: Torque map of the aeroelastic simulations as function of wind speed u and turbulence intensity TI.

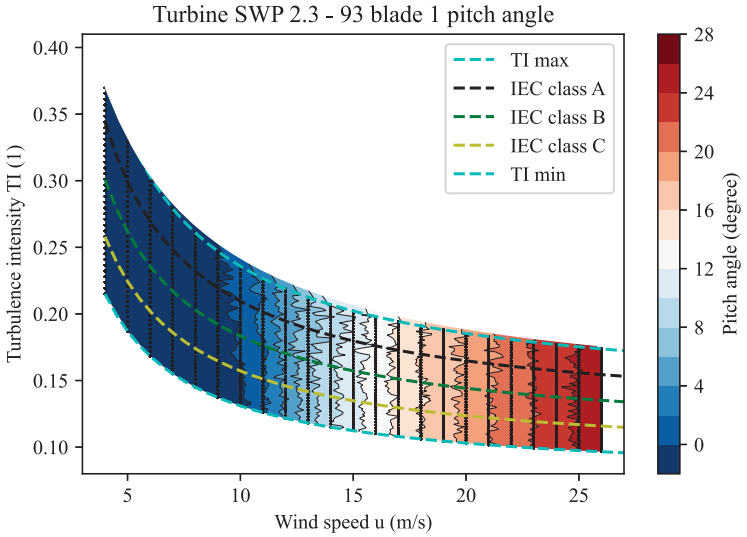

Figure 5.9: Pitch angle map of the aeroelastic simulations as function of wind speed u and turbulence intensity TI.

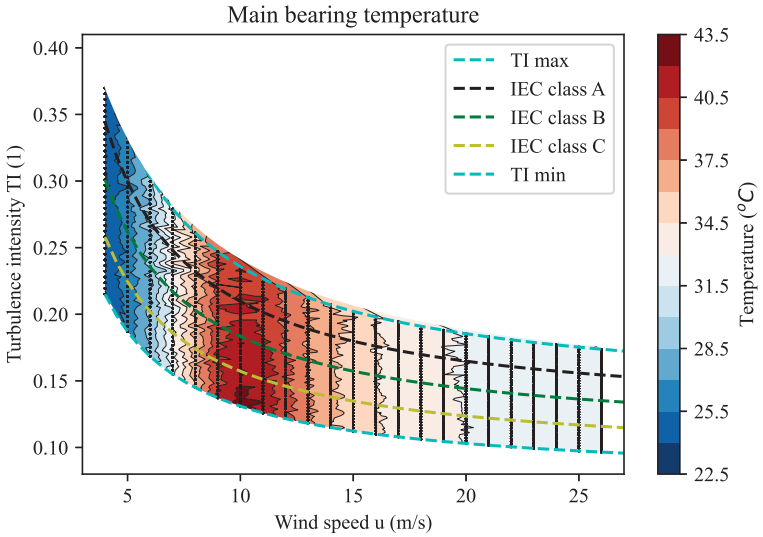

Figure 5.10: Map of estimated main bearing temperature as determined from a simple heat model including the friction heating and the main bearing equivalent loads of the aeroelastic simulations as function of wind speed u and turbulence intensity TI. It is assumed that the main bearing ambient temperature is $T_{amb} = 20\ ^oC$ since the SWT2.3 - 93 turbines for offshore wind farms are equipped with a dehumidification system keeping the nacelle temperature above this temperature. The cleanliness of the grease is assumed fully clean with $e_C = 1.0$ according to ISO 281.

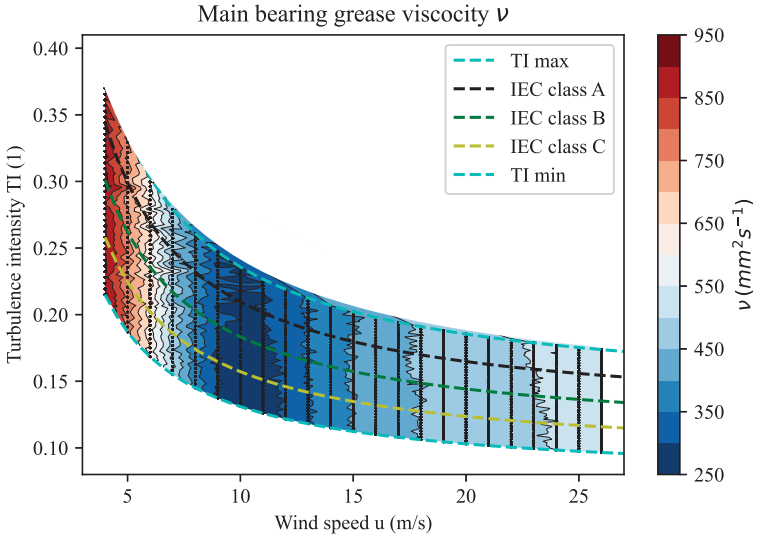

Figure 5.11: Map of expected kinematic viscosity of the grease of the main bearing as described by the ISO 281 standard and solving for the main bearing temperature of the aeroelastic simulations as a function of wind speed u and turbulence intensity TI. The cleanliness of the grease is assumed fully clean with $e_C = 1.0$ according to ISO 281.

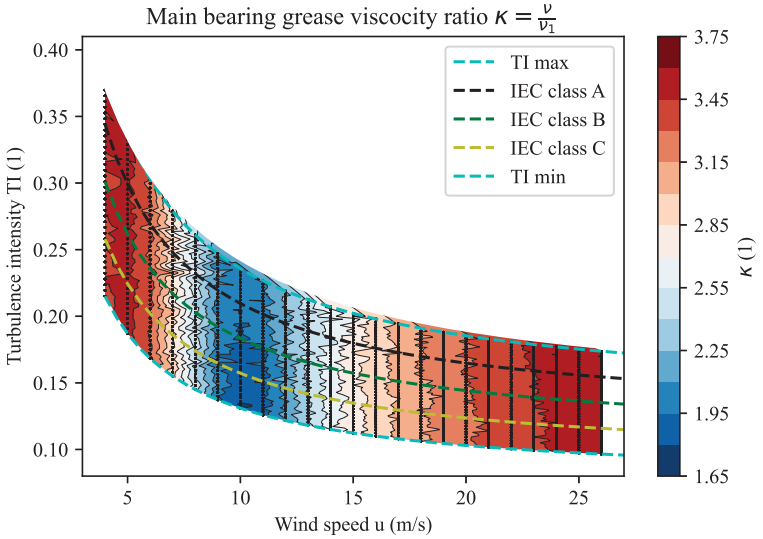

Figure 5.12: Map of kinematic viscosity ratio $\kappa = \frac{\nu}{\nu_1}$ of the grease of the main bearing as described by the ISO 281 standard and solving for the main bearing temperature of the aeroelastic simulations as a function of wind speed u and turbulence intensity TI. The cleanliness of the grease is assumed fully clean with $e_C = 1.0$ according to ISO 281.

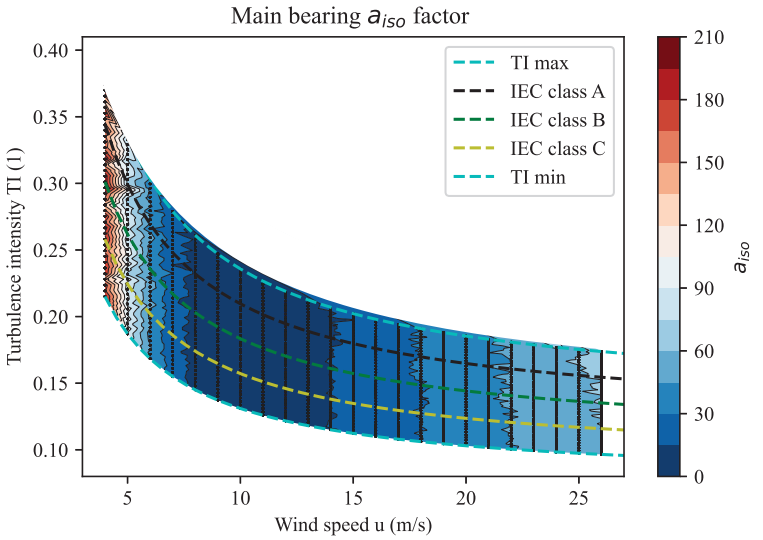

Figure 5.13: Map of expected life modification factor due to operation a_{iso} of the grease of the main bearing as described by the ISO 281 standard and solving for the main bearing temperature of the aeroelastic simulations as a function of wind speed u and turbulence intensity TI. The cleanliness of the grease is assumed fully clean with $e_C = 1.0$ according to ISO 281. The a_{iso} is recommended limited at $a_{iso} < 50$, but full range is shown here to show the trend in the entire parameter space of the aeroelastic simulations.

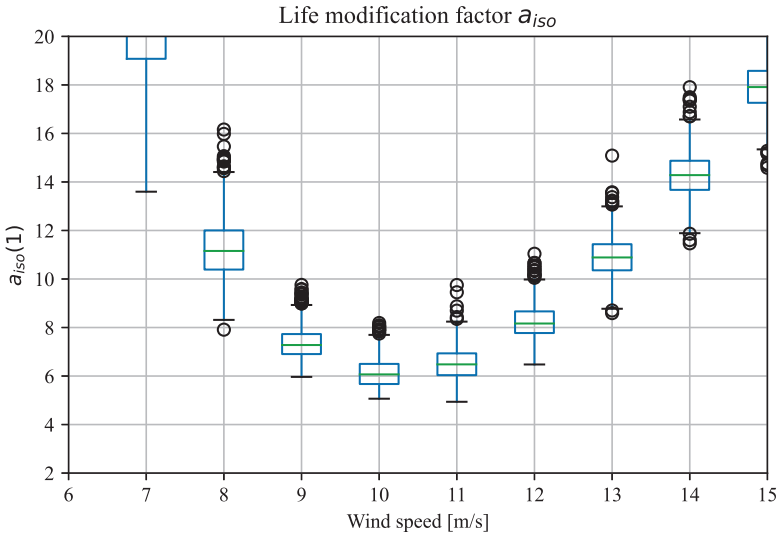

Figure 5.14: Region of low expected life modification factor due to operation a_{iso} of the grease of the main bearing as described by the ISO 281 standard. The cleanliness of the grease is assumed fully clean with $e_C = 1.0$ according to ISO 281. It is noted that the a_{iso} is larger than a factor of 6 for all time-series and the resulting modified main bearing life is increased by this factor.

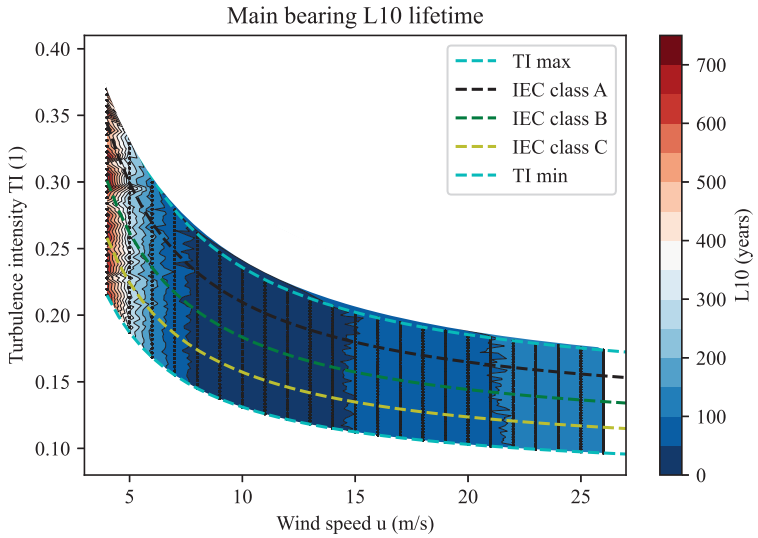

Figure 5.15: Basic L10y lifetime of the main bearing as a function of the wind speed u and the turbulence intensity TI.

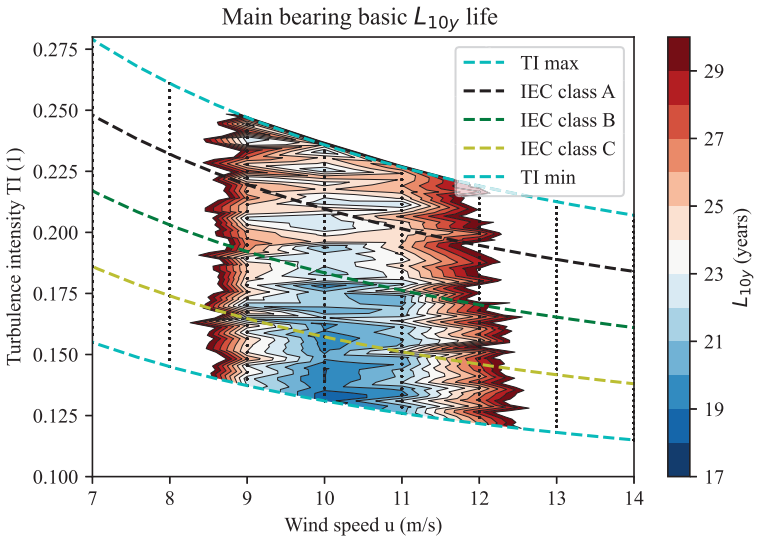

Figure 5.16: Focus on the smaller values of the basic L_{10y} lifetime of the main bearing as function of the wind speed u and the turbulence intensity TI.

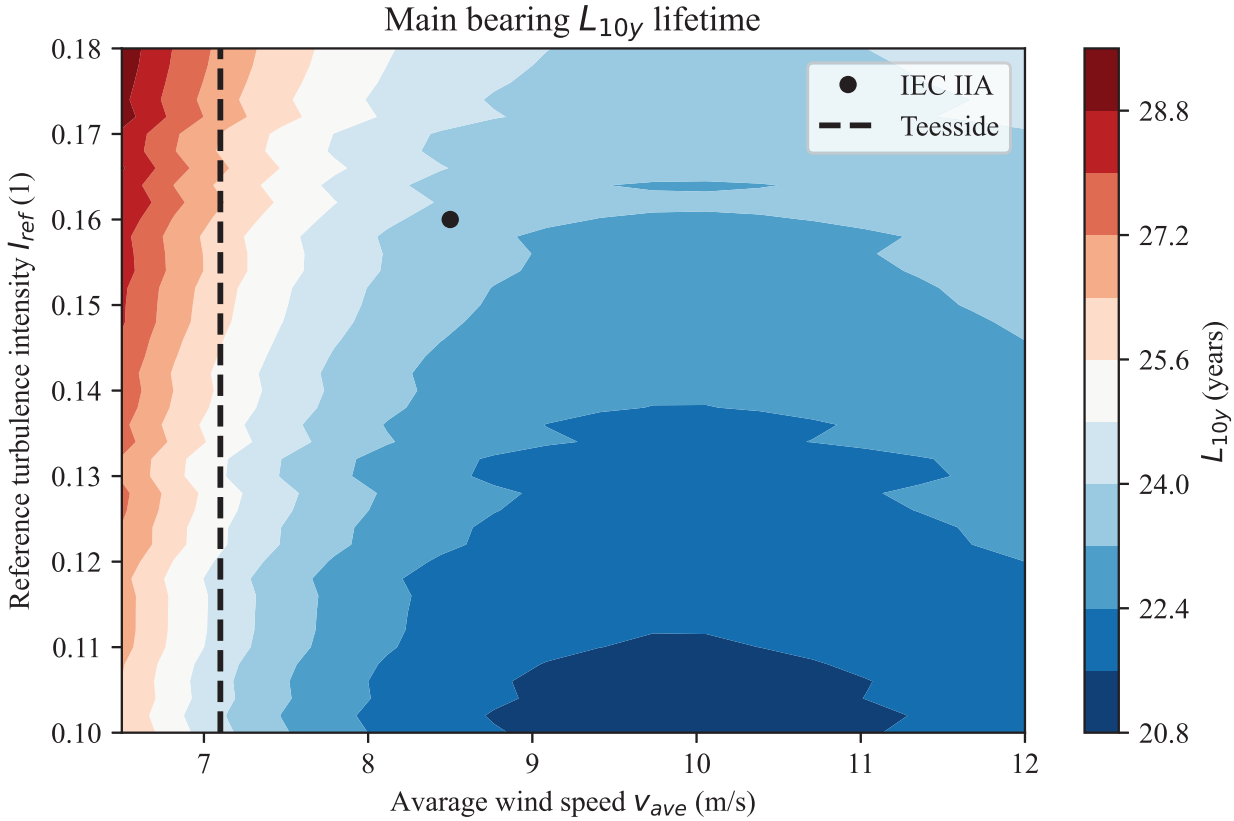

Figure 5.17: Map of the main bearing combined L_{10y} life from the aeroelastic model of the SWT 2.3 - 93 turbine as a function of the characteristic parameters of the wind environment in terms of the average wind speed v_{ave} and the IEC Normal Turbulence Model reference turbulence intensity I_{ref}. The IEC design wind class IIA of the SWT2.3 - 93 turbine has been indicated by a dot and the average wind speed $v_{ave} = 7.1$ m/s of the Teesside wind farms is marked by a dashed line.

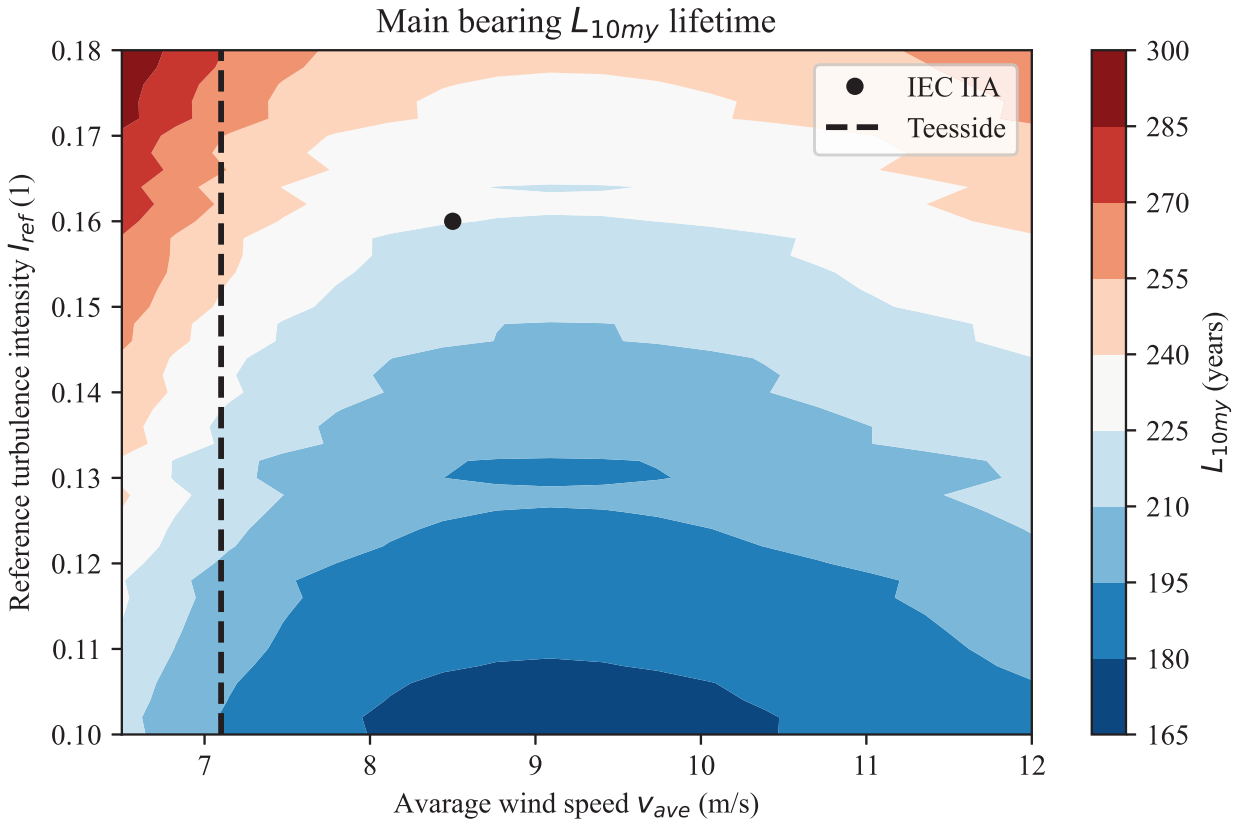

Figure 5.18: Map of the main bearing modified L_{10my} lifetime, where the a_{iso} modification factor has been taken into account.The IEC design wind class IIA of the SWT2.3 - 93 turbine has been indicated by a dot and the average wind speed $v_{ave} = 7.1$ m/s of the Teesside wind farms is marked by a dashed line. The grease cleanliness factor has been assumed to be the cleanest possible with $e_C = 1.0$ according to ISO 281.

5.2 Teesside wind farm environmental characteristics

The SCADA data of the Teesside wind farm has been analysed according to the methodology section and Figure 5.19 shows the wind speed distribution of the 27 turbines as observed in the period 2015-2018. It is seen that the distributions appear similar across the entire wind farm and the differences are quantified by the fitted Rayleigh average wind speed obtained by fitting the distribution function of eq.(4.1) to the histograms. The maximum wind speeds observed in the SCADA data ranges between 27-34 m/s as seen from the max points in Figure 5.19. A bump in the wind speed distributions is observed at $u \approx 3$ m/s and this is believed to be caused by the shadowing of the turbine rotor of the cup anemometer sitting behind the rotor and also to the cut-vind wind speed $v_{cut-in} = 4$ m/s of the SWT 2.3 - 93 turbines.

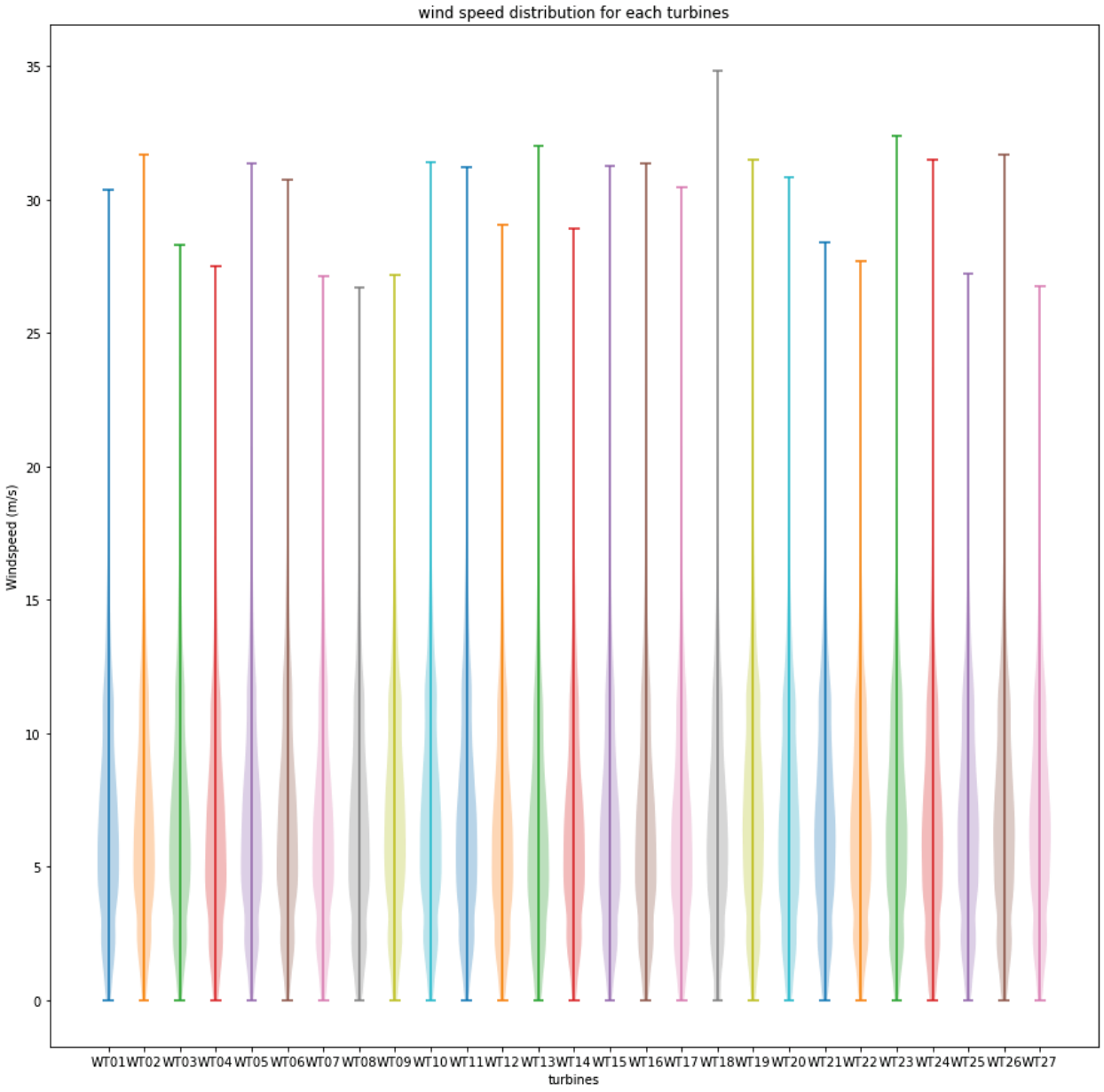

Figure 5.19: Comparison of the wind speed distributions of the 27 wind turbines of the Teesside wind farm as illustrated in Figure 2.1.

The average wind speed v_{ave} as obtained from the Rayleigh fit to the SCADA data is shown in 5.20, where it is clearly observed that turbine 11-18 show lower average wind speed most likely caused by the wakes from the turbines at the edges of the wind farm. The farm average of the average wind speeds is close to previously reported value of $v_{ave,Teesside} = 7.1m/s$ Papatzimos et al. (2018).

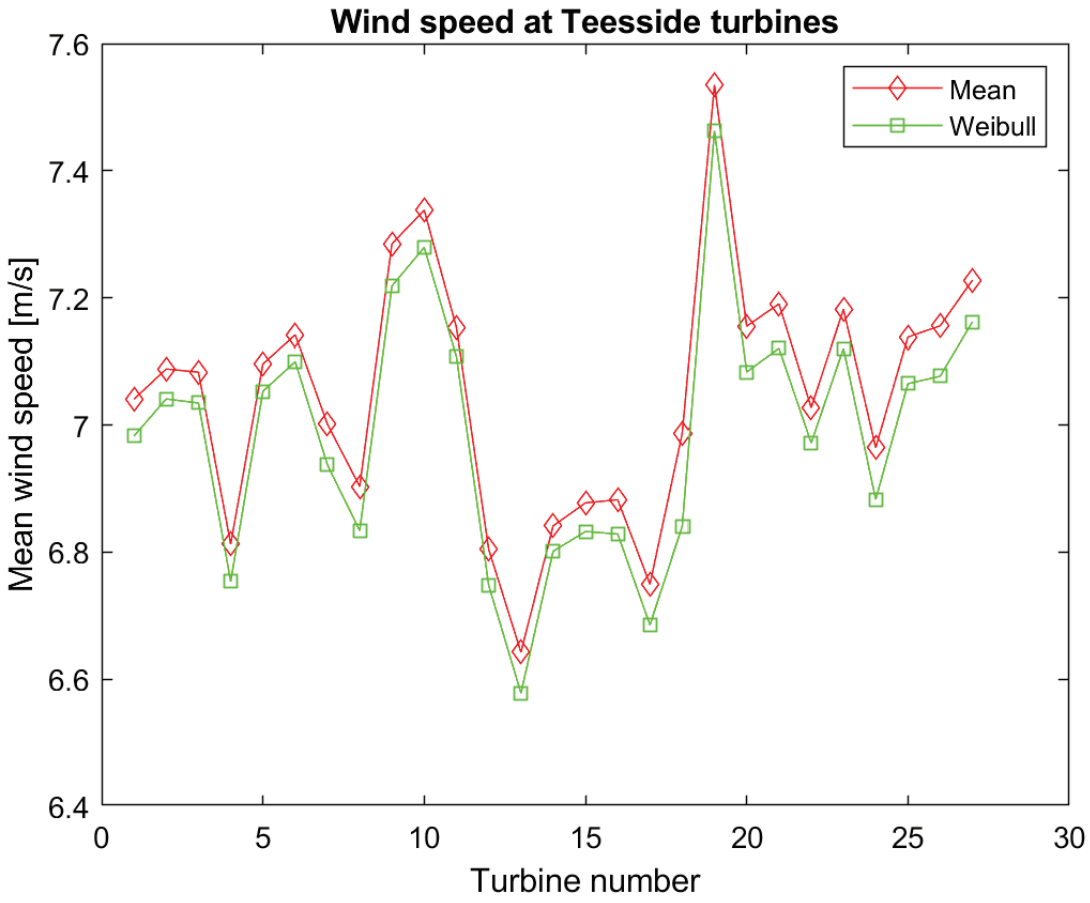

Figure 5.20: Plot of the fitted average wind speed v_{ave} as given by the Rayleigh distribution in eq. (4.1) of the 27 wind turbines of the Teesside wind farm as illustrated in Figure 2.1.

The distribution of the standard deviation of the wind speed of the wind turbines of the Teesside wind farm is shown in Figure 5.21. Again it is seen that most of the turbines are behaving in the same way, but with the exception of turbine WT13 showing values exceeding above 2 m/s. The maximum values of the wind speed standard deviation are in the range 5.3 - 7.8 m/s. The origin of these larger values of wind turbine WT13 can not be explained by a simple measuring error of the anemometer of the turbine and it has been decided to report the value for further analysis and not to discard this point.

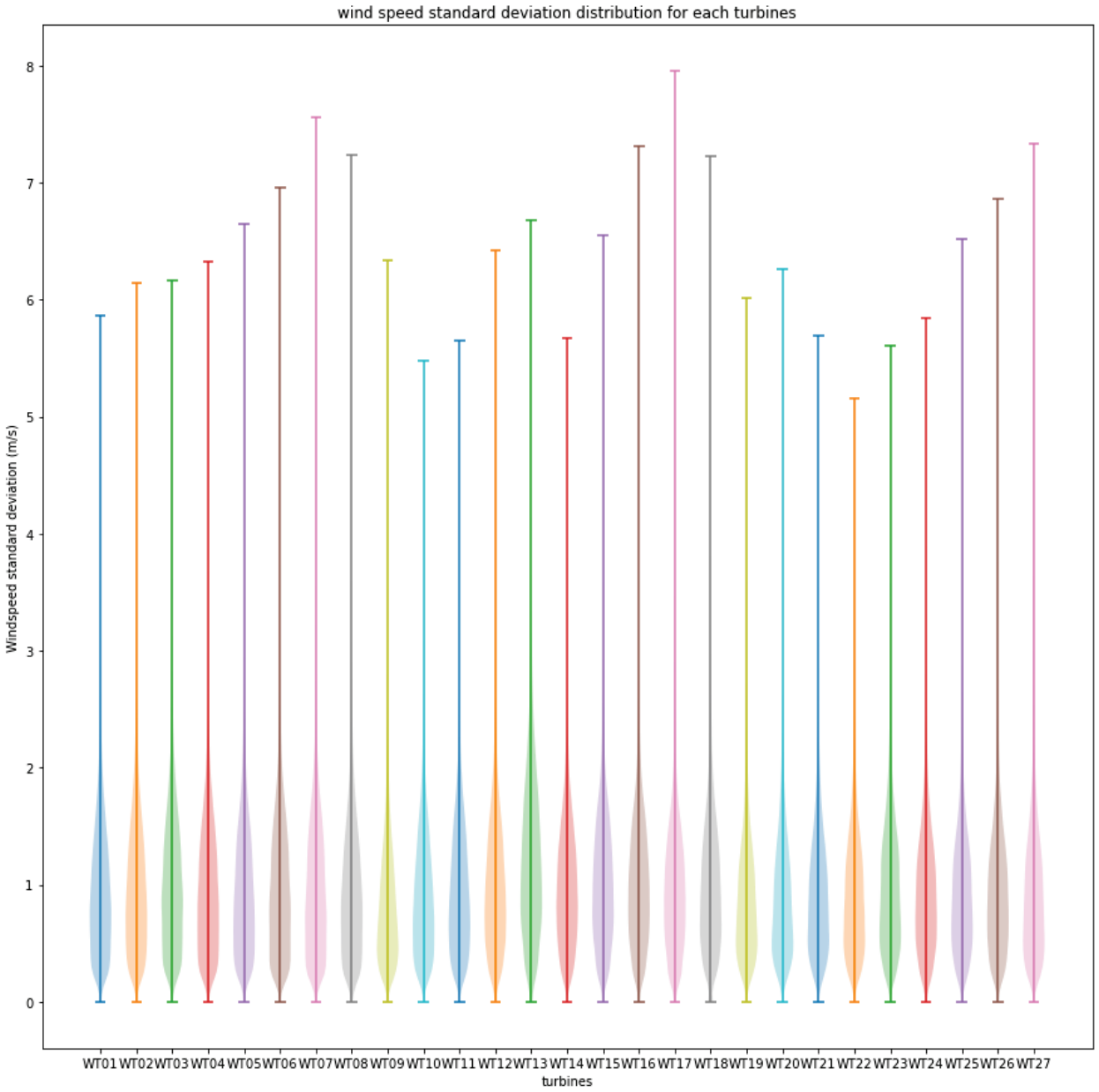

Figure 5.21: Comparison of the wind speed standard deviation of the 27 wind turbines of the Teesside wind farm as illustrated in Figure 2.1 showing the position of the turbines named WT1-27.

In order to quantify the local wind environment of the Teesside wind turbines then four different methods were applied to fit the normal turbulence distribution to the SCADA data of the Teesside wind farm. The first two methods use the definition of the IEC normal turbulence model as given by eq.(4.2)

$$\sigma_{1,fit} = \begin{cases} \mathrm{I}_{ref,fit}(0.75u + b_{fixed}) & b_{fixed} = 5.6\,m/s \\ \mathrm{I}_{ref,fit}(0.75u + b_{fit}) \end{cases} \tag{5.1}$$

where u is the wind speed of the measurements and σ_1 is determined as the 90 % quantile of the SCADA measurements. $I_{ref,fit}$ and b_{fit} are the obtained fitting parameters characterizing the wind conditions. Since eq.(5.1) is a linear function then a linear fitting routine is used to perform the fit and will be denoted as "linear" in the following plots.

The last two methods use the definition of turbulence intensity as given by eq.(4.3)

$$TI_{fit} = \begin{cases} \frac{\mathrm{I}_{ref,fit}(0.75u+b_{fixed})}{u} & b_{fixed} = 5.6\,m/s \\ \frac{\mathrm{I}_{ref,fit}(0.75u+b_{fit})}{u} \end{cases} \tag{5.2}$$

Again u is the wind speed of the measurements and the turbulence intensity TI is determined as the 90 % quantile of the SCADA measurements. From eq.(5.2) it is seen that a non-linear fitting routine is needed to obtain the fitting parameters and the results will be denoted "non-linear" in the following plots.

Figure 5.22, Figure 5.23 and Figure 5.24 shows the linear fits to the standard deviation of the wind speed for the 9 upper most turbines, the 9 middle turbines and the 9 lower turbines of the Teesside wind farm and the turbine ID numbers are taken from Figure 2.1. Thus the left hand column of the plots of Figure 5.22 are facing the land and consists of the turbines WT19-WT21, the middle column are the turbines WT10-WT12 in the middle of the wind farm and the last column consist of the turbines WT01-WT03 facing the seaside of the Teesside wind farm. In general terms one can say that the IEC standard deviation of the wind speed with a fixed b $=$ 5.6 m/s value is fitting the behavior of the turbines facing the sea quite well, but the slope is changing for the turbines facing land. It is expected that wake interaction between the turbines will alter the local wind conditions away from the ideal IEC normal turbulence model and a perfect fit is therefore not expected.

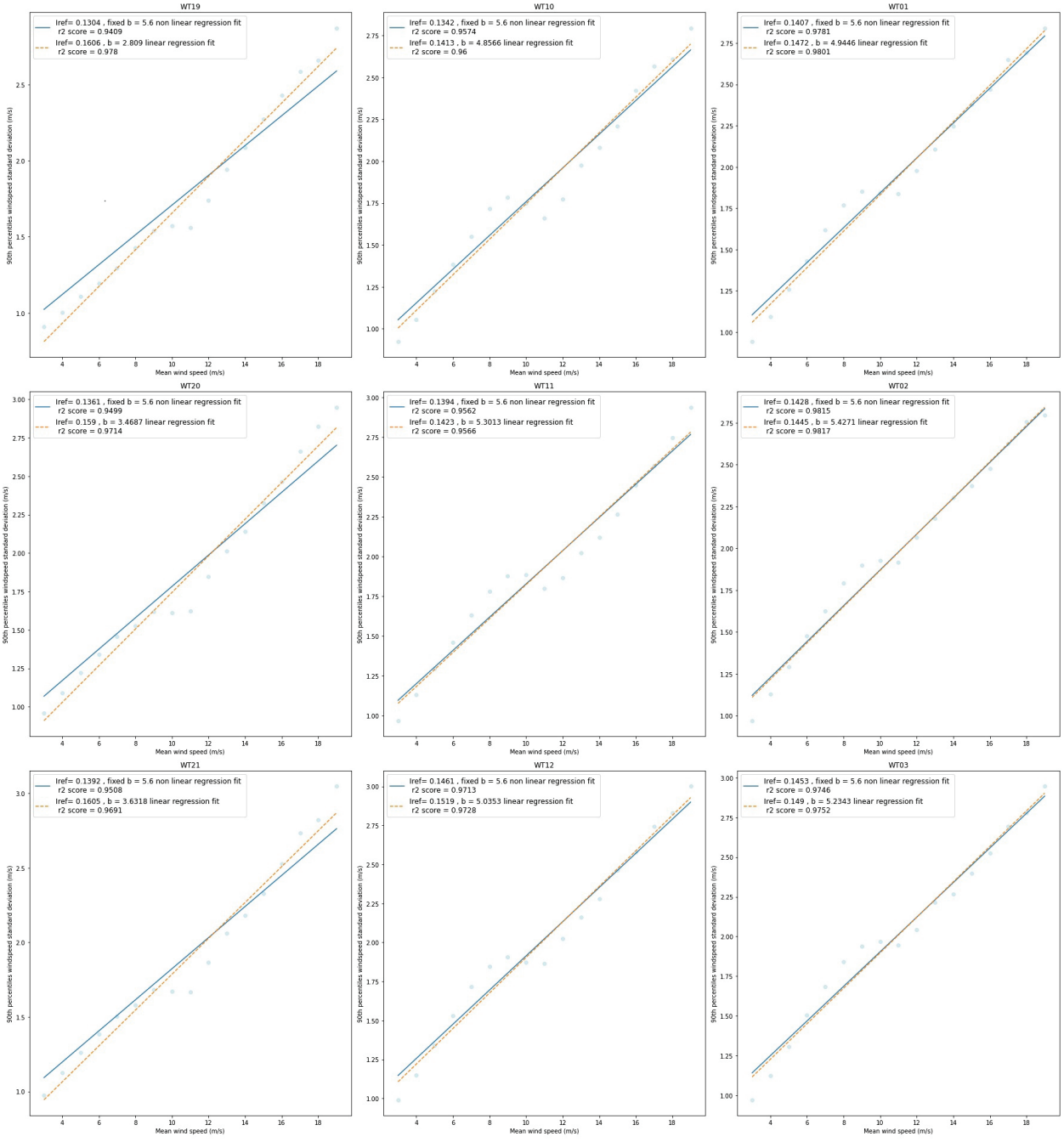

Figure 5.22: Plot of the 90 % quantile of wind speed standard deviation as function of the average wind speed of upper 9 wind turbines of the Teesside wind farm as illustrated in 2.1. The linear fits are shown by the full lines.

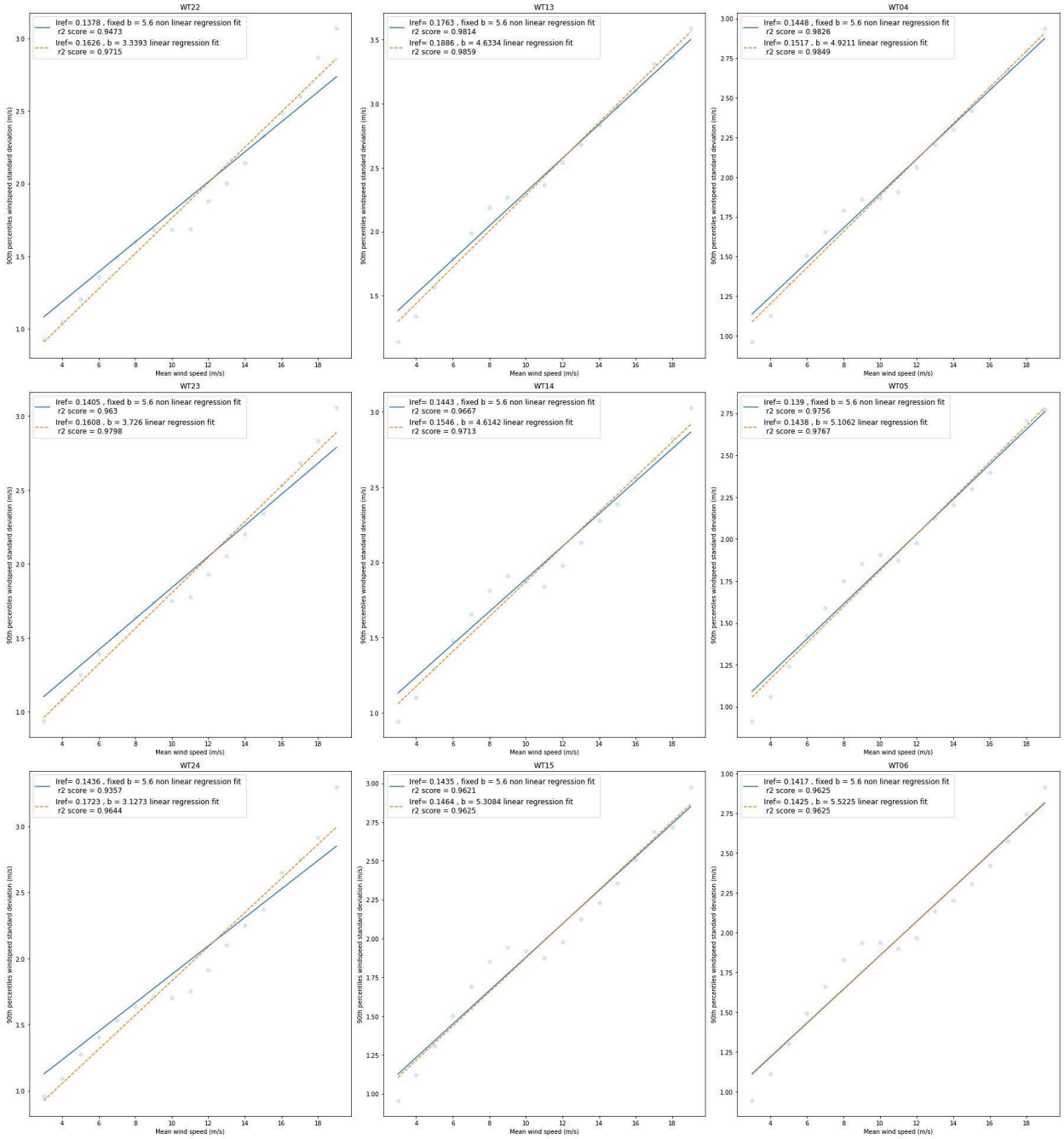

Figure 5.23: Plot of the 90 % quantile of wind speed standard deviation as function of the average wind speed of mid 9 wind turbines of the Teesside wind farm as illustrated in 2.1. The linear fits are shown by the full lines.

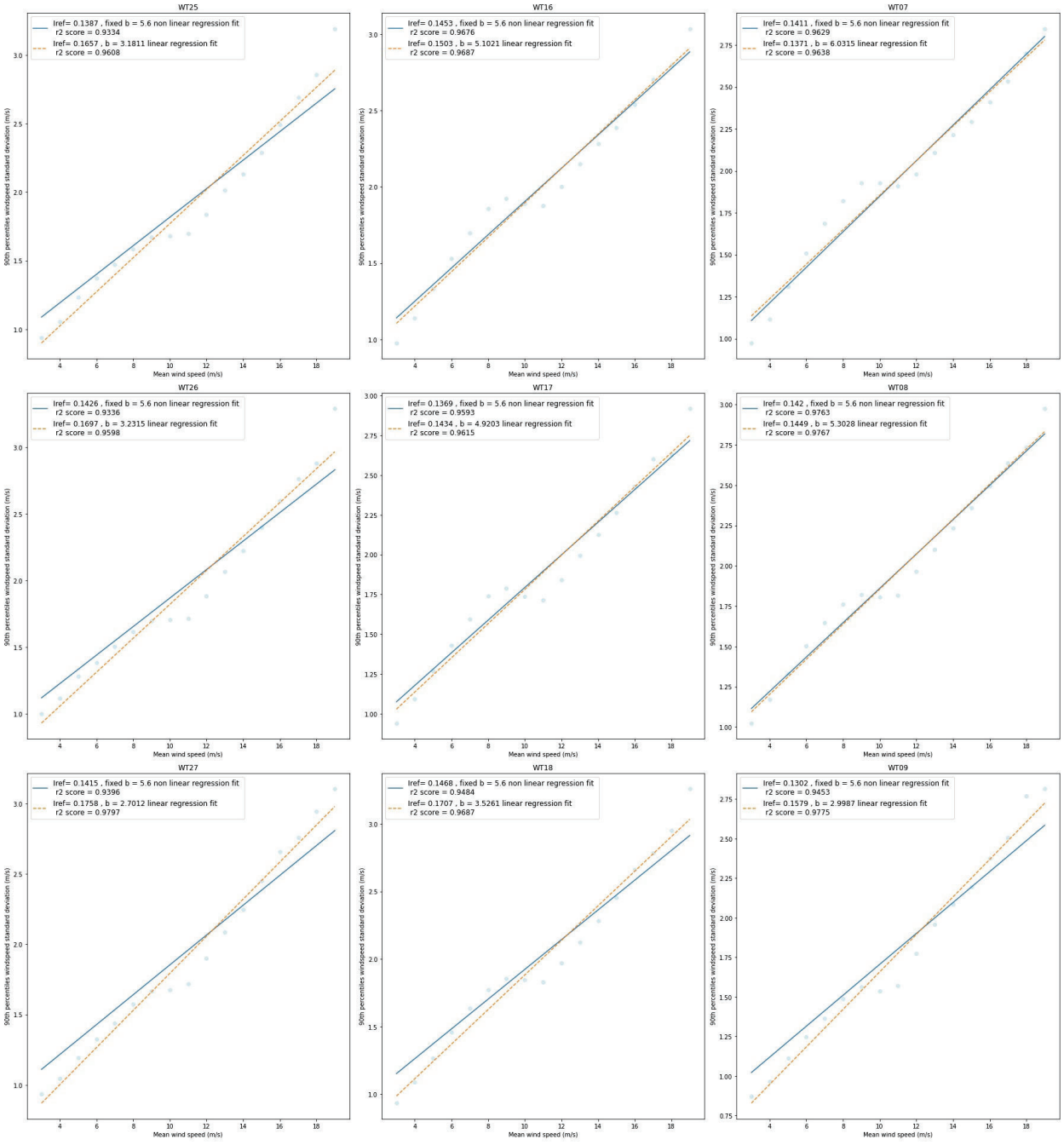

Figure 5.24: Plot of the 90 % quantile of wind speed standard deviation as function of the average wind speed of the lower 9 wind turbines of the Teesside wind farm as illustrated in 2.1. The linear fits are shown by the full lines.

The results of the fitting method based on the turbulence intensity as outlined in eq.(5.2) are shown in Figure 5.25, Figure 5.26 and Figure 5.27. Again the upper 9, the middle 9 and the lower 9 turbines of Teesside wind farm are shown and the non-linear fits to the 90 % quantile of the turbulence intensity are shown as solid lines. It is generally seen that the non-linear fit with both the reference turbulence intensity I_{ref} and the b value considered as fitting parameters are describing the turbulence intensity distributions the best and that fixing $b = 5.6\,m/s$ is not providing as good fits.

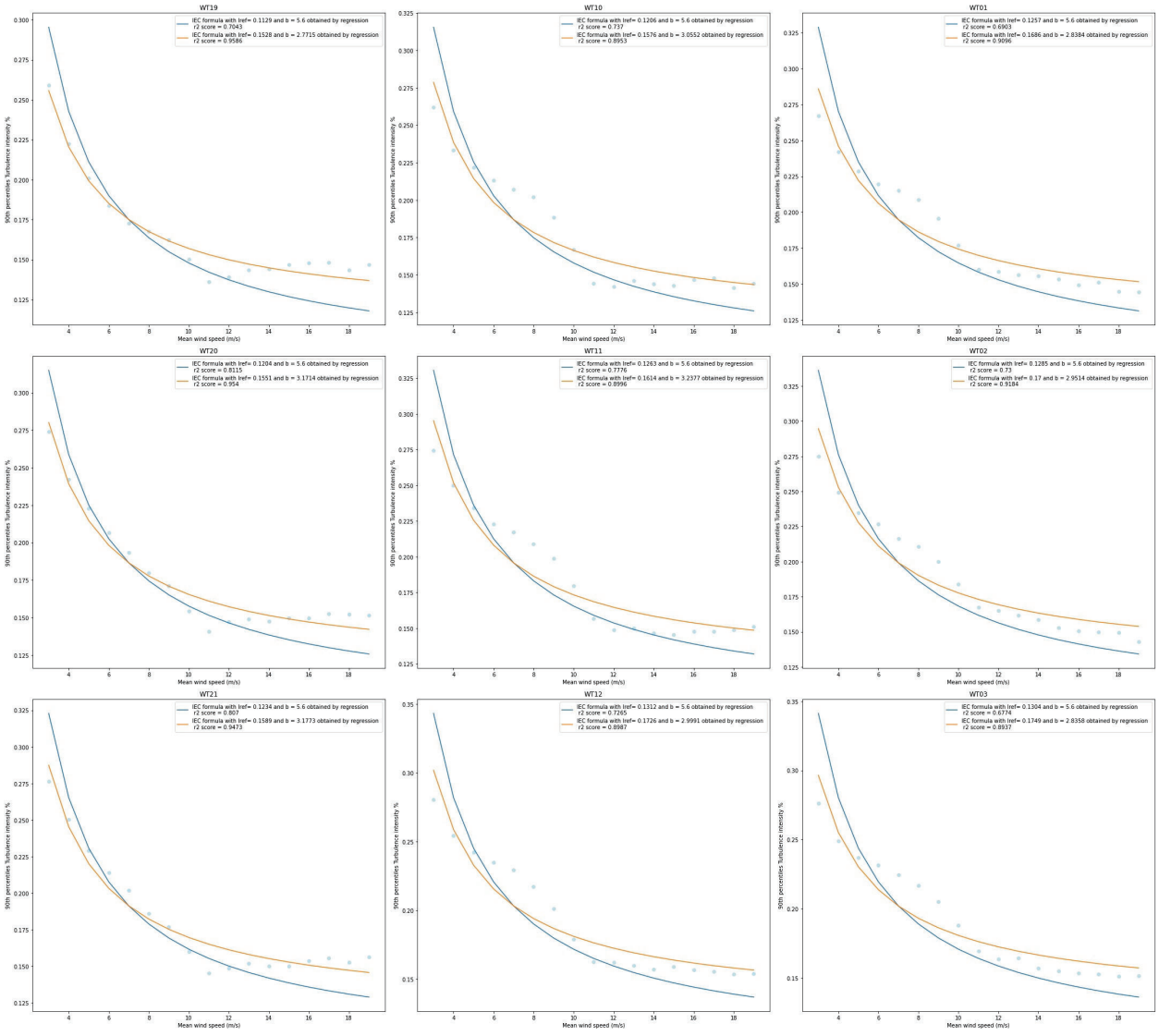

Figure 5.25: Plot of the 90 % quantile of the turbulence intensity TI as function of the average wind speed of the upper 9 wind turbines of the Teesside wind farm as illustrated in 2.1. The non-linear fits are shown by the full lines.

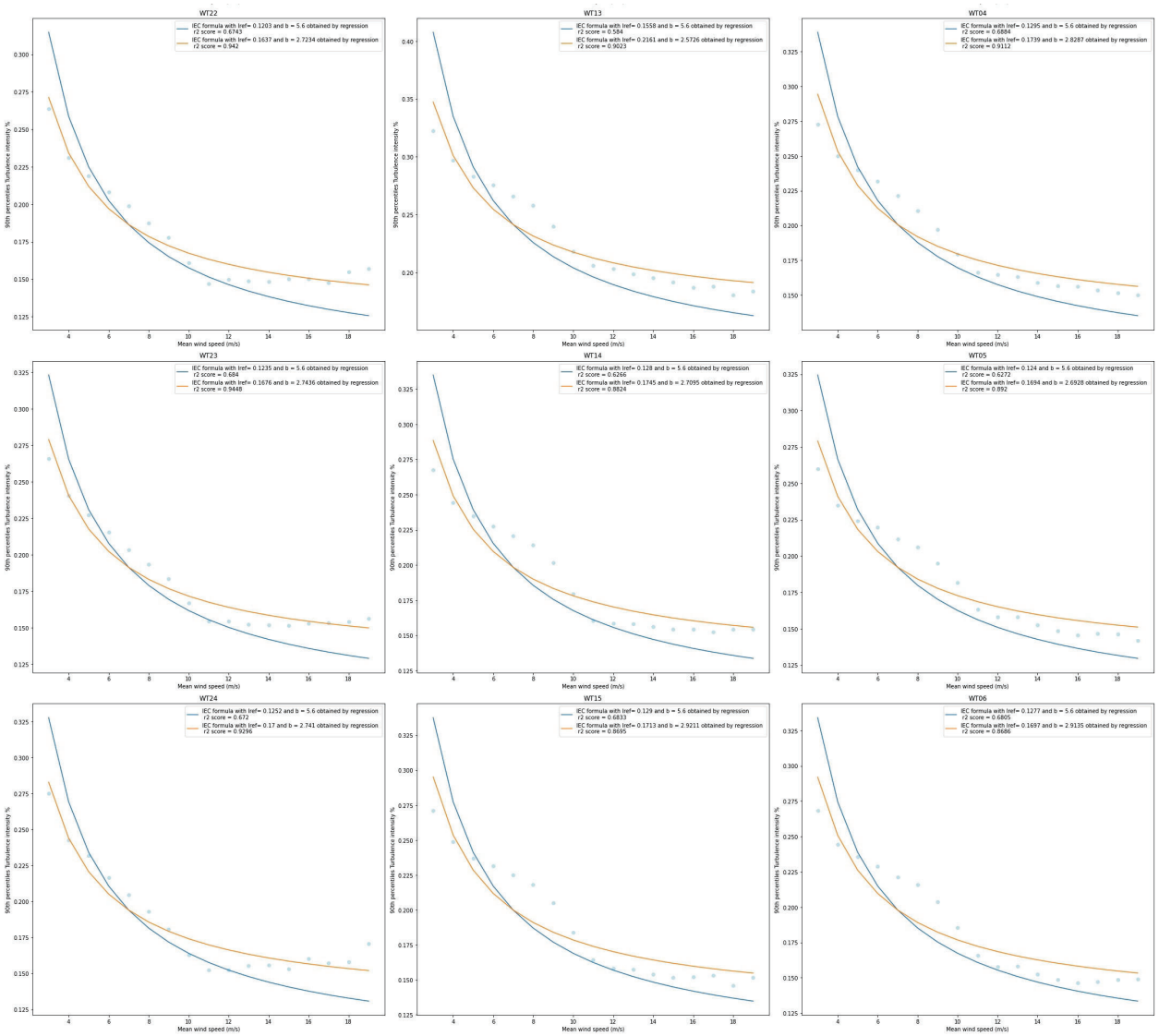

Figure 5.26: Plot of the 90 % quantile of the turbulence intensity TI as function of the average wind speed of the mid 9 wind turbines of the Teesside wind farm as illustrated in 2.1. The non-linear fits are shown by the full lines.

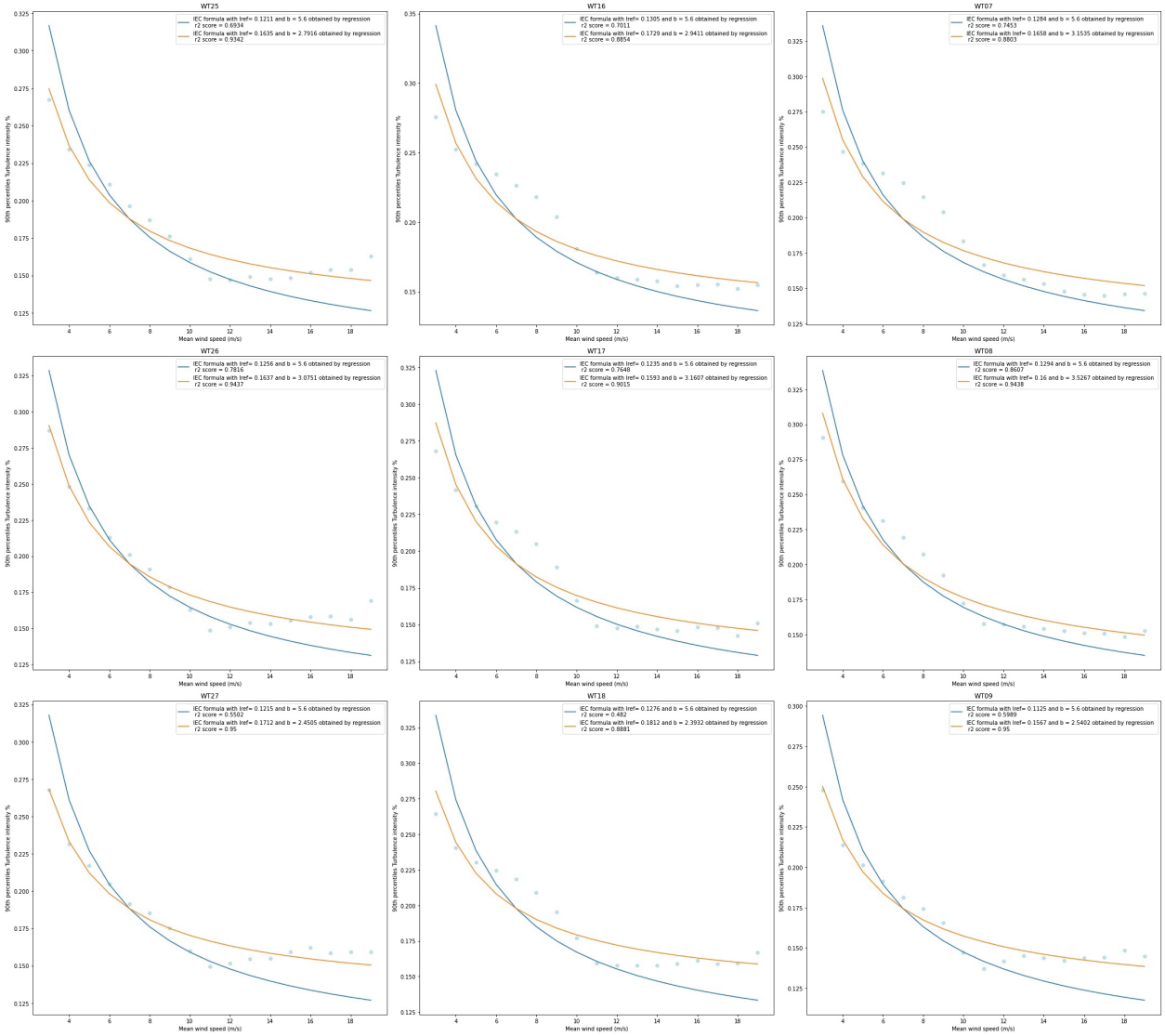

Figure 5.27: Plot of the 90 % quantile of the turbulence intensity TI as function of the average wind speed of the lower 9 wind turbines of the Teesside wind farm as illustrated in 2.1. The non-linear fits are shown by the full lines.

The turbulence model fitting parameters obtained from the Teesside wind speed time series are summarized in Figure 5.28 showing the reference turbulence intensities I_{ref} and Figure 5.29 showing the b-value of the normal turbulence models. From Figure 5.28 it is seen that the four curves of I_{ref} are offset by about ± 0.02 around an average level of $I_{ref} = 0.14$. From the fitted b-values shown in Figure 5.29 it is seen that the expected IEC level of $b = 5.6\,m/s$ is observed for the first 18 turbines (except WT9), whereas the b value decreases to around $b_{fit,linear} \approx 3.0 - 3.5\,m/s$ for turbine 9 and WT19-WT27. The non-linear fit with the b-value as fitting parameter shows values in the range of $b_{fit,non-lin} \approx 3.0 - 3.5\,m/s$.

The fitting procedure has shown that the use of a fixed b-value equal to 5.6 m/s in the normal turbulence model is not providing the best fit to the observed distributions, and that the nonlinear version with b considered as a fitting parameter provides a better fit. In order to interpret the wind conditions of the Teesside wind farm, it is desired to feed the wind conditions into the main bearing life model as outlined in the previous chapters. Since the simple normal turbulence model was used for the aeroelastic simulations of the main bearing loads, one will also have to restrict the choice of the b-value to b = 5.6 m/s according to the IEC standard for consistency. Secondly, it was observed that the linear fit with b = 5.6 m/s seems to provide a better fit than the non-linear method, and the I_{ref} values of the red curve of Figure 5.28 are used for creating a main bearing life map of the Teesside wind farm.

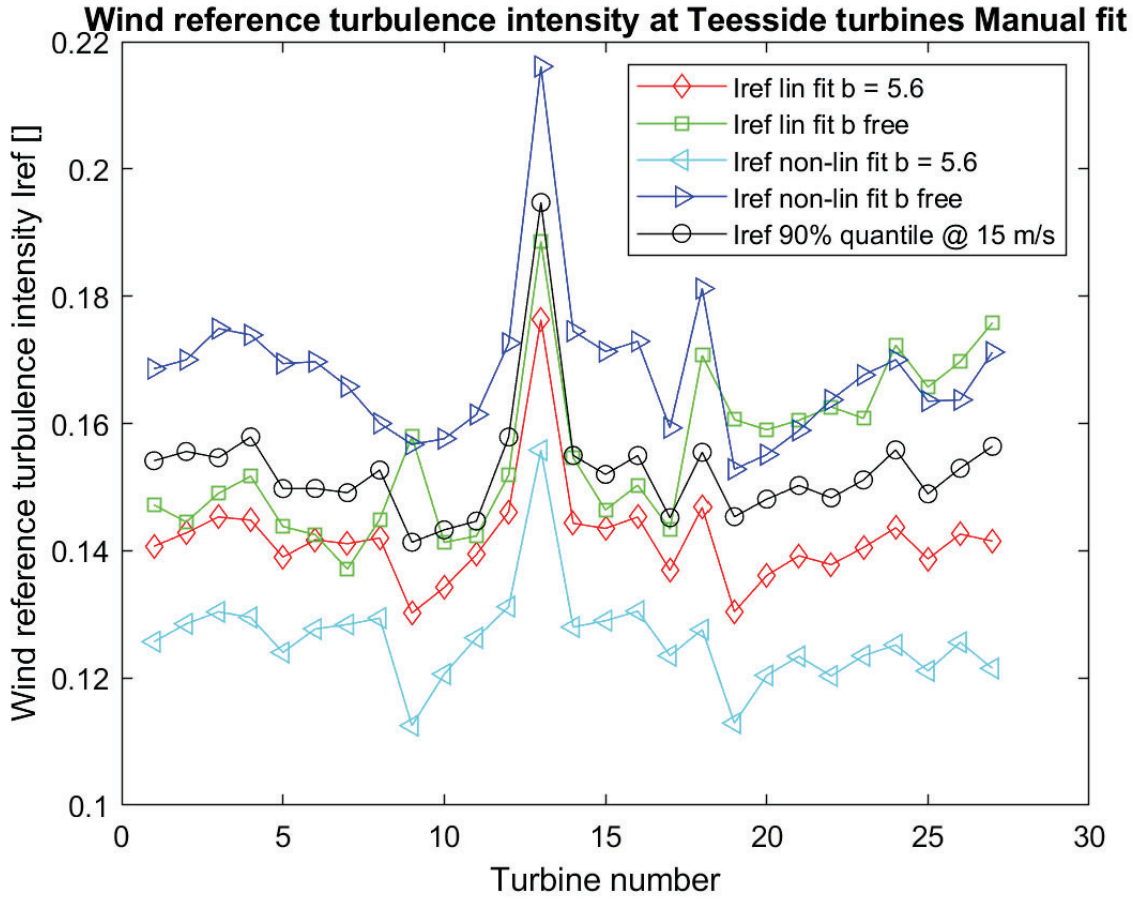

Figure 5.28: Plot of the reference turbulence intensity I_{ref} of the 27 wind turbines of the Teesside wind farm as illustrated in 2.1.

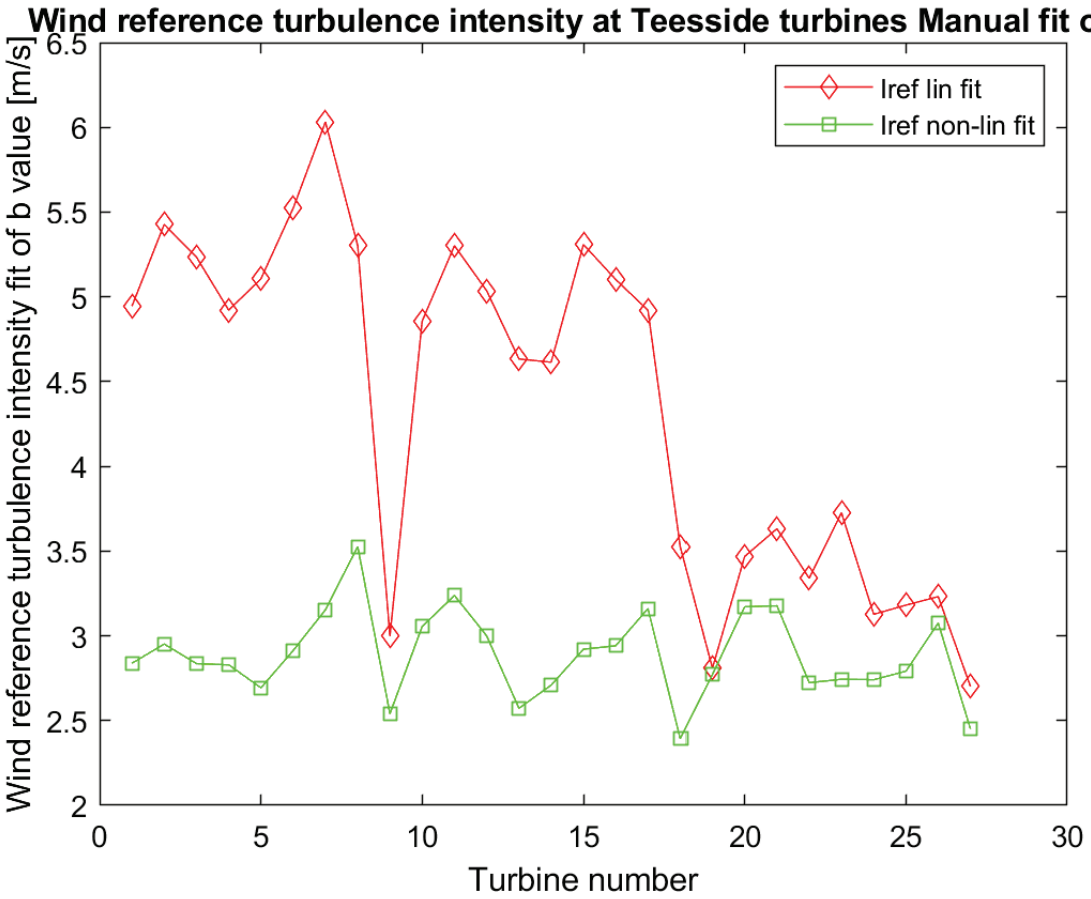

Figure 5.29: Plot of the b-value fitting parameter of the normal turbulence model of the 27 wind turbines of the Teesside wind farm as illustrated in 2.1.

5.3 Teesside wind farm main bearing life map

The analysis of the average wind speed v_{ave} and the reference turbulence intensity I_{ref} of the IEC normal turbulence model can feed this into the main bearing life model of the Teesside wind turbines of Figure 5.17 and Figure 5.18. In order to illustrate the input, Figure 5.30 is showing a contour map of the average wind speed of the different turbines in the coordinate system normalized by the rotor diameter of the SWT 2.3 - 93 m turbines with $D_{rotor} = 93\,m$. Similarly, the reference turbulence intensity I_{ref} is shown in Figure 5.31 over all turbine positions. The resulting main bearing life map of the Teesside wind farm is shown in Figure 5.32 in terms of the basic L_{10y} lifetime. A similar map of the modified L_{10my} lifetime based on the a_{iso} factor as given by Figure 5.13 shows lifetimes considerably longer than the 25 year design lifetime of the turbine and is shown in Figure 5.33. Here, the predicted main bearing L10m lifetimes are ranging between 210 to 280 years, because the lowest a_{iso} factor is approximately 8. Figure 5.34 shows the lifetime of the main bearing of the Teesside wind turbines WT1-WT27. It is observed that the two corner turbines WT9 and WT19 have a main bearing lifetime of 23.5 years and 23.8 years whereas the turbine column WT1-8 and WT20-27 have a lifetime of approximately 25 years. The center column of turbines WT14-18 shows lifetimes of approximately 25.5 years and the outlier of WT13 shows a lifetime of approximately 29 years. It has not possible to explain the deviation of WT13 from the analysis of the SCADA data.

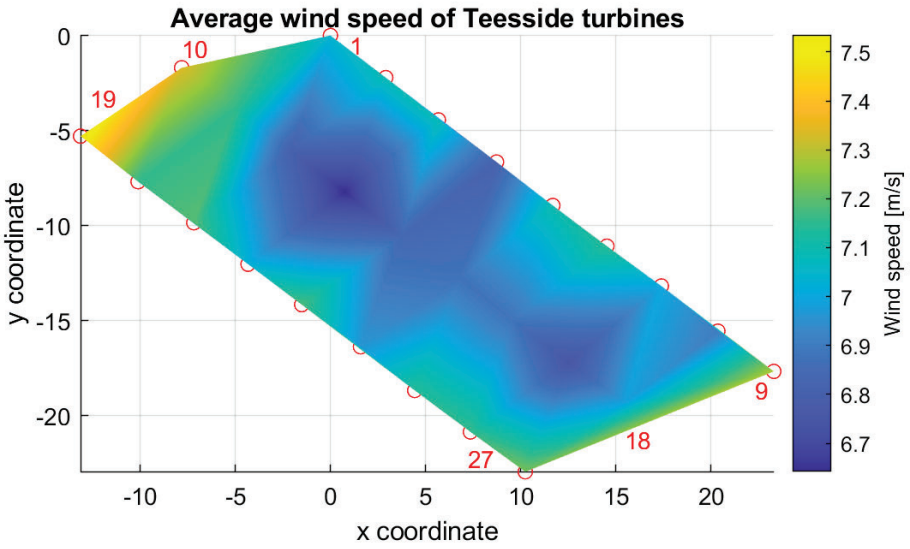

Figure 5.30: Distribution of average wind speed v_{ave} at the position of wind turbines of the Teesside wind farm.

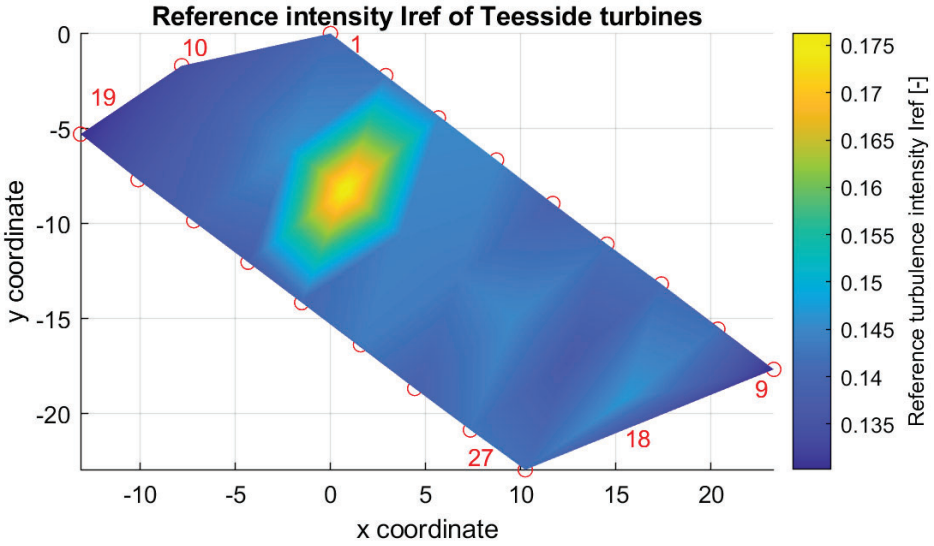

Figure 5.31: Distribution of reference turbulence intensity I_{ref} at the position of wind turbines of the Teesside wind farm.

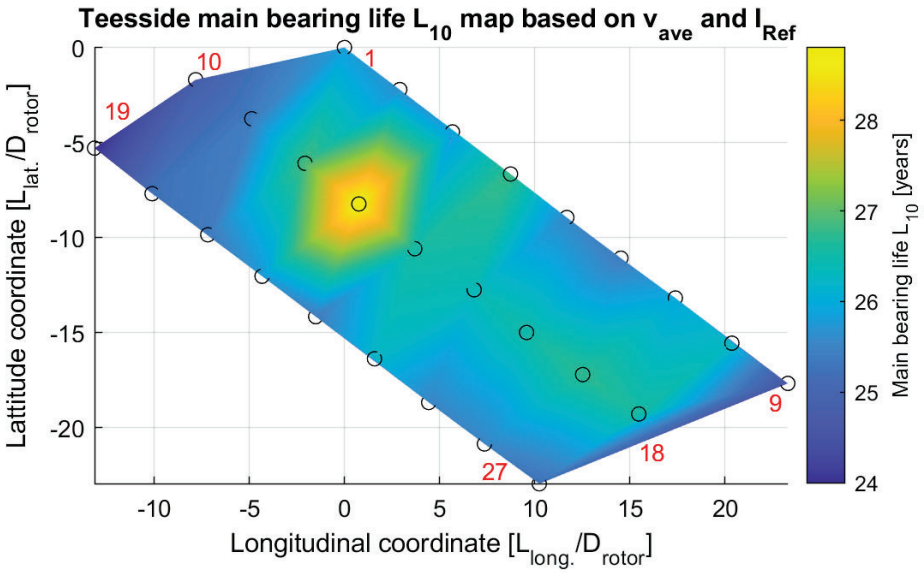

Figure 5.32: Main bearing L_{10y} life map of the Teesside wind farm based on the average wind speed v_{ave} of Figure 5.30 and the reference turbulence intensity I_{ref} of Figure 5.31. The coordinate positions of the wind turbine WT1-WT27 at the edges of the wind farms are indicated by the red numbers.

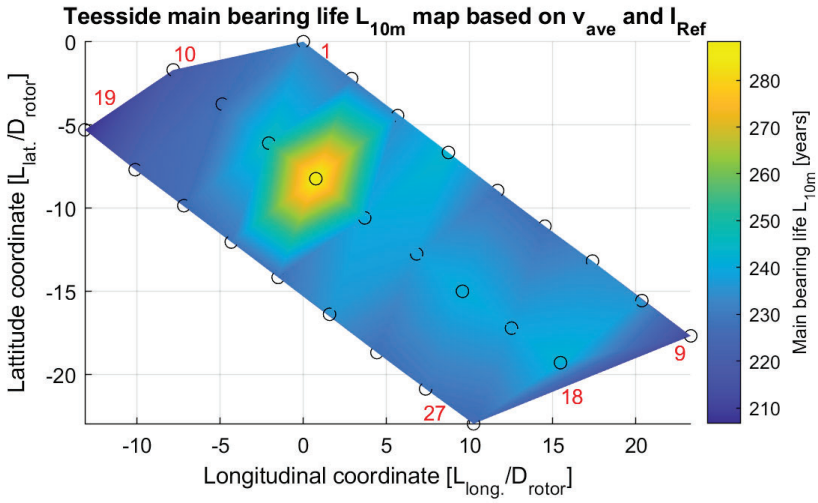

Figure 5.33: Main bearing L_{10my} life map of the Teesside wind farm based on the average wind speed v_{ave} of Figure 5.30 and the reference turbulence intensity I_{ref} of Figure 5.31. The life modification factor of system approach a_{iso} based on clean grease ($e_C = 1$) has been multiplied onto the basic L_{10} lifetime. The coordinate positions of the wind turbine WT1-WT27 at the edges of the wind farms are indicated by the red numbers.

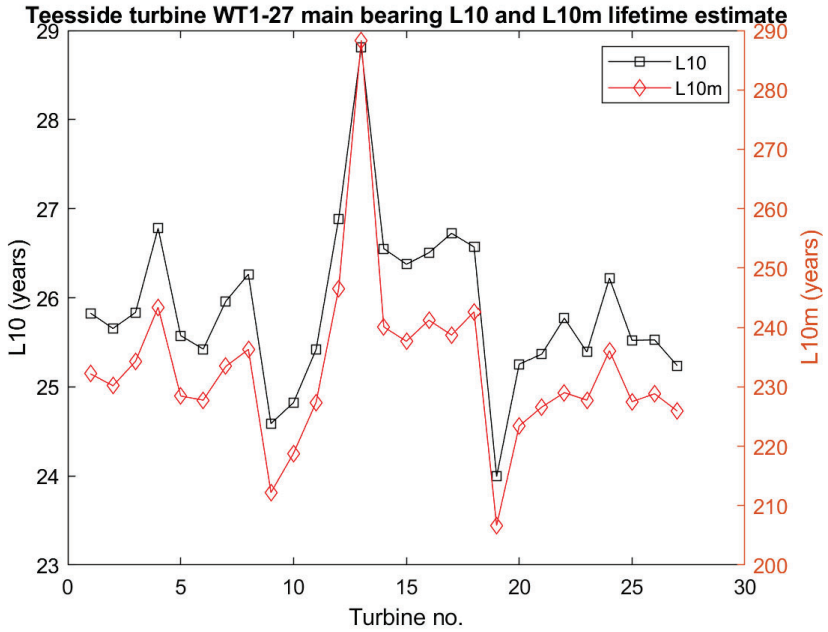

Figure 5.34: Main bearing L_{10y} and L_{10my} lifetime of the Teesside turbines WT1-WT27.

5.4 Probability propagation of Teesside main bearing failures

The Teesside main bearing lifetime map of Figure 5.32 and 5.33 can be re-scaled from the L_{10} lifetime denoting a 10 % failure fraction of an identical set of bearings operated under the same conditions and into a failure fraction of n % using the Weibull function outlined in eq.(3.13). From the Teesside lifetime map it was seen that the average L_{10} lifetime of the Teesside wind turbines is approximately 25 years and the simple interpretation of this is that 10 % of the bearings of the Teesside wind farm are expected to have failed after 25 years of operation. Thus 10 % of the 27 turbines correspond to about 3 main bearing failures are expected after 25 years of operation.

Figure 5.35 shows the cumulative distribution function of the main bearing time to failure L_{ny}. If we treat the 27 bearings as statistically independent and with identically distributed properties following the said distribution, we can approximately estimate the combined likelihood of observing failures on wind farm level. The probability corresponding to 1 out of 27 turbines failing has been indicated by a dashed horizontal line at $F = 1/27 = 3.7\%$. Similarly, the failure levels of 2 and 3 out of 27 turbine main bearings have been shown as well as the failure level of 10 % corresponding to the L_{10} lifetime. From the Weibull distribution of Figure 5.35 one can see that the first main bearing failure at the Teesside wind farm is expected between year 12-15, the second between year 20-23 and the third between year 25-32. It is not possible to say which of the 27 bearings that will fail and this is showing that the role of the condition monitoring system is to point out the weak bearings out of the 27.

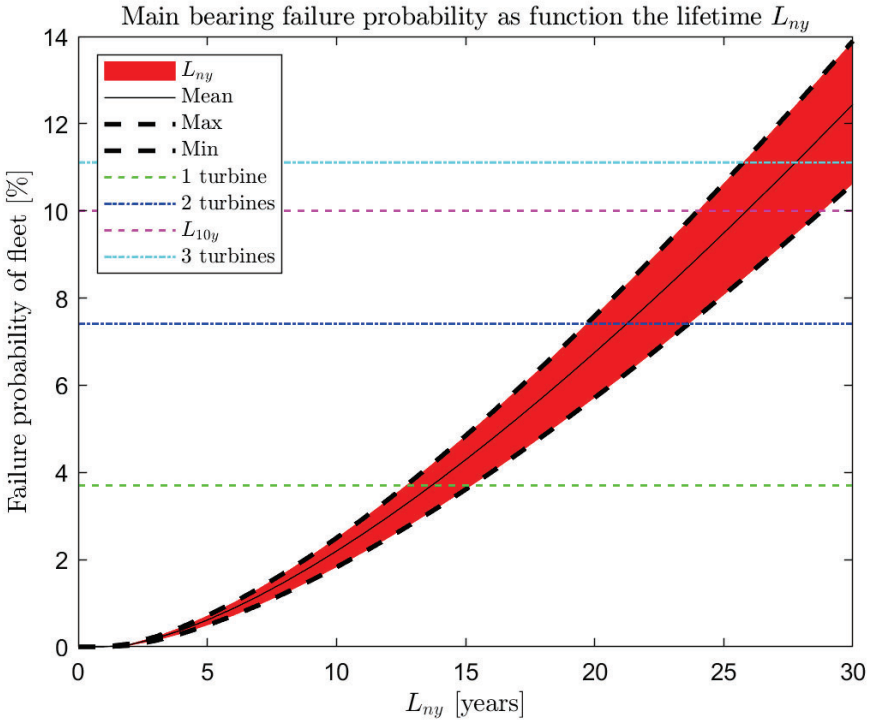

Figure 5.35: Failure probability of the main bearing of the Teesside wind turbines as function of the L_{ny} lifetime. The dashed lines indicate the cumulative failure probability equivalent to 1 out of 27, 2 out of 27 and 3 out of 27 main bearings failing in the Teeside wind farm. The 10 % cumulative failure probability corresponds to the L_{10} lifetime as given in Figure 5.34

The life modification factor for reliability a_1 and the life modification factor for system approach a_{iso} can then be used to scale the L_{10} lifetime to the modified L_{nm} lifetime for a failure level of n % and taking into account the modification of the grease cleanliness factor e_C and operation temperature. Figure 5.36 shows the modified lifetime of the main bearing and it is now seen that the first main bearing is expected to fail between year 110 and year 150, the second between year 170 and year 240 and the third between year 220 and year 310. This lifetime is much longer than the design life time of the offshore turbine often specified to be 25 years. Thus as long as the grease is kept clean in the main bearing then all the main bearings are expected to last considerably longer than the design lifetime of 25 years.

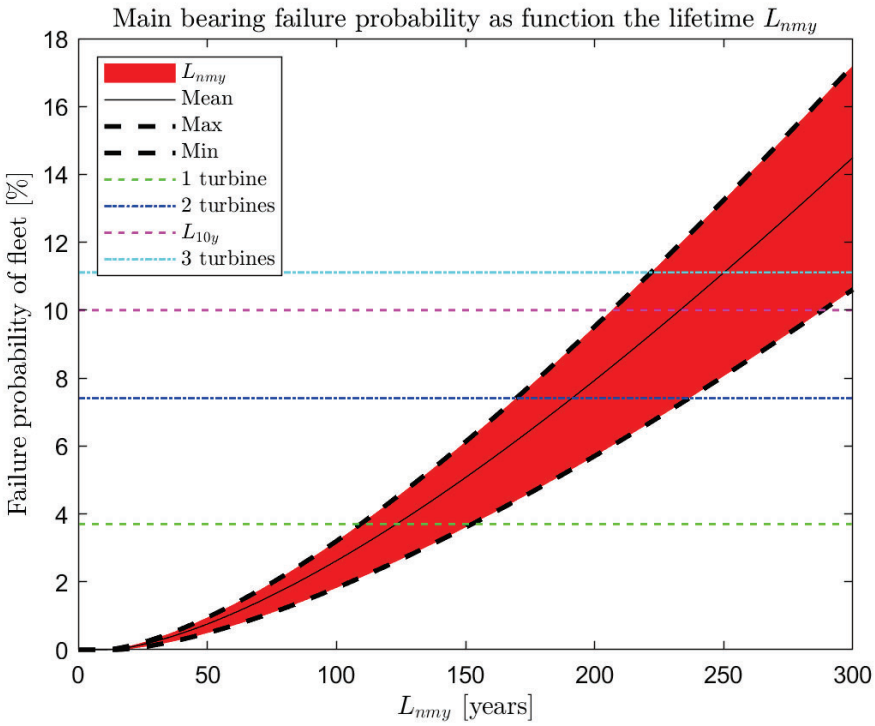

Figure 5.36: Failure probability of the main bearing of the Teesside turbines as function of the L_{nmy} modified lifetime. The horizonthal dashed lines indicate the failure probability equivalent to 1 out of 27, 2 out of 27 and 3 out of 27 main bearings failing in the Teeside wind farm. The 10 % failure probability corresponds to the L_{10my} lifetime as given in Figure 5.34

The failure rate of the main bearings of the Teesside wind farm can now be determined using eq.(3.14) and eq.(3.15) from the basic L_{10} lifetime. This is shown in Figure 5.37 and it is observed that the failure rate reaches 0.5 %/year after 25 years of operation or 0.15 main bearing failures per year.

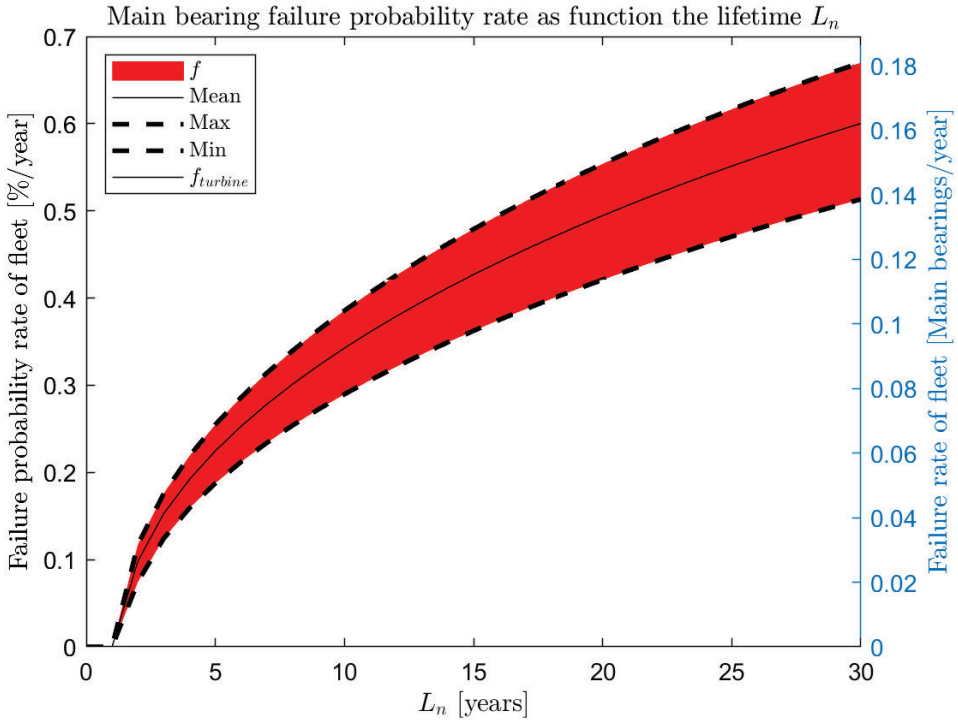

Figure 5.37: Expected annual failure rate of the main bearing of the Teesside turbines as function of the L_{ny} modified lifetime. The main bearing failure rate as determined from eq.(3.15) is shown on the right hand axis.

The failure rate is however reduced considerably when the modified lifetime L_{nm} is used as shown in Figure 5.38. It is seen that the failure rate is approximately 0.015 %/year after 25 years, since the a_{iso} is taken into account for the calculation of the modified lifetime and it is assumed that the grease is operated as fully clean with $e_C = 1$.

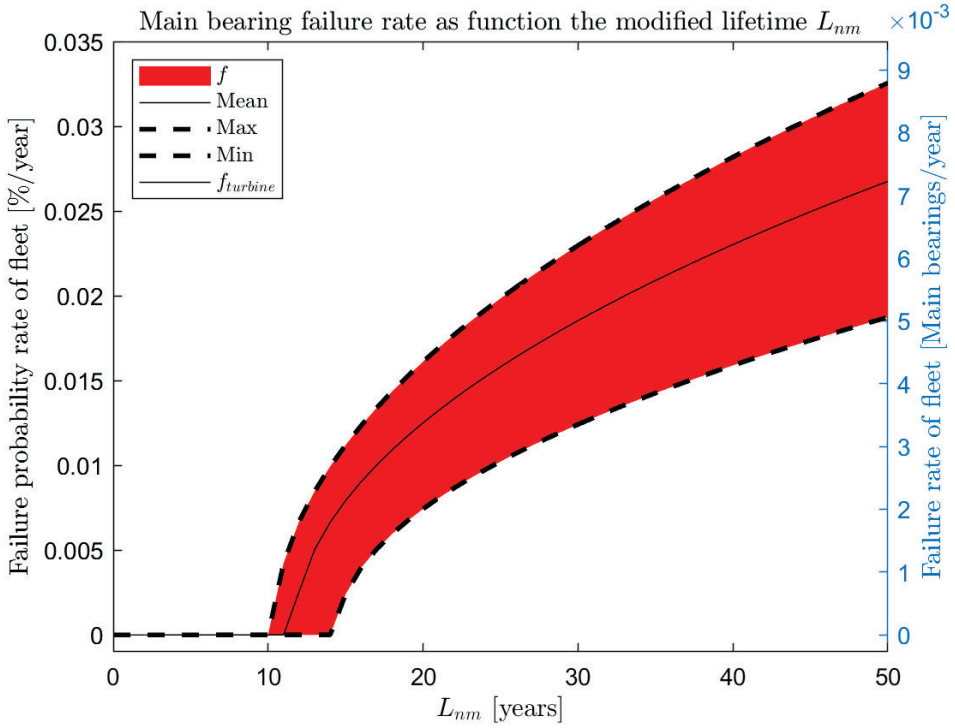

Figure 5.38: Failure probability rate of the main bearing of the Teesside turbines as function of the L_{nmy} modified lifetime. The main bearing failure rate as determined from eq.(3.15) is shown on the right hand axis.

6 Discussions

The physics-based lifetime model of the FAG 230/800 main bearing of the SWT 2.3 - 93 turbines of the Teesside offshore wind farm has been established using publicly available information about the components obtained from second hand spare part trading companies like SparesInMotion. This approach has been used in order to provide a public description of as many input parameters as possible in order to allow others to reproduce the results. The downside of this approach is that many uncertainties in terms of exact dimensions had to be accepted and were estimated based on engineering judgment. The ranges of input parameters like the wind speed and turbulence intensities of the SWT 2.3 - 93 turbine were investigated in a rather large parameter space compared to the properties of the Teesside wind farm, because the Teesside wind farm turbulence parameters were not widely known from the start of the project. This might have demanded more resources than necessary for performing the analysis of the Teesside wind farm, but it is believed that the model analysis on the main bearing lifetime of the SWT 2.3 - 93 turbine can be transferred to other offshore wind farms using this turbine type if the wave loads are not playing a dominating role. The main challenges that have been faced during the formulation of the physics-based life model have been related to the validity of applying the ISO 281 standard to the wind turbine main bearing and to the interpretation of the ISO 281 results.

The first challenge of collecting the information about the main bearing and the grease was solved by using public sources as described above. It is possible that alternative main bearings and greases can be used, but the FAG 230/800 bearing lubricated with a Klüberplex BEM 41-301 grease is suggested as a good representation of the main bearing component. The second

challenge to establish the loads of the SWT 2.3 - 93 turbines was solved by using an Hawc2 aeroelastic model of the turbine that had been compared with internal aeroelastic simulations of EDF. Thus, already for Hiperwind deliverable D5.1 (Remigius et al., 2023), estimations of the basic lifetime L_{10} of the main bearing could be determined. A simple thermal model of the main bearing was provided in Deliverable D5.1 and the temperature of the main bearing was estimated to reach $T_{MB} \approx 73\,^oC$ at rated wind speed resulting in expected a_{iso} factor decreasing below 1 and thereby flagging out a modified lifetime of the main bearing lower than the basic lifetime. From the literature, it was known that the main bearing temperature of normal operating wind turbines is expected to be below $T_{MB,normal} \approx 50^oC$ and this indicated that the simple thermal model was over-estimating the main bearing temperature. This analysis is very similar to the discussion of Kenworthy et al. Kenworthy et al. (2024) reporting that initial attempts to use the ISO 281 also over-predicted the main bearing temperature of wind turbines. As a response, it was planned to make a comparison with the Teesside main bearing temperature of the SCADA data, and an exchange of additional SCADA data was done with EDF. Secondly the thermal model of the main bearing was elaborated to include a heat flow both through the steel surrounding the outside of the main bearing leading the heat to the bed frame of the turbine as well as the heat flow through the main shaft and to the hub flange. This has been described in Hiperwind Deliverable D5.3 (Abrahamsen et al., 2024), where the thermal model is shown to predict the main bearing temperature of the SWT 2.3 - 93 turbines quite well. Since the temperature range of the thermal model prediction provides a reasonable estimate of the main bearing temperature, it is now possible to investigate the resulting a_{iso} factor from the model. Figure 5.13 and Figure 5.14 shows the a_{iso} factor predicted from the aeroelastic simulations feeds into the ISO 281 equations combined with the thermal model. A minimum $a_{iso} \approx 6$ and ranging up to 210 is observed around the rated wind speed of the turbine and at low wind speed near the cut-in wind speed respectively. This estimation is assuming a completely clean grease with a contamination factor of $e_C = 1$. A consequence of the predicted a_{iso} is that the modified lifetime of the bearing becomes very long and in the order of hundreds of years, and one could state that the model is suggesting that the SWT 2.3 - 93 turbine main bearings should be indestructible when installed in the Teesside wind farm. The paper of Kenworthy et. al. have found similarly high lifetime of a 240 / 630 main bearing for a 1.5 MW GE turbines Kenworthy et al. (2024).

The a_{iso} map of Figure 5.13 is however based on the assumption of a perfectly clean grease and if one starts to decrease the contamination factor e_C towards zero then the a_{iso} will also reduce considerably below 1 and the life of the main bearing will decrease below the basic lifetime L_{10}. This decrease might end up being an accelerated process, where the friction heating of the bearing is increasing and might cause a change of the chemical composition of the grease due to an increased temperature as well as an increased accumulation of metal debris in the grease. There are also a large number of external factors affecting the main bearing lifetime, such as the tightness of the main bearing seals to both prevent water and dirt from leaking in, as well as grease from leaking out of the main bearing. The re-greasing system pumping in fresh grease into the main bearing might also malfunction or the piping system could clog up on both the input as well as the output ports of the main bearing. So in order to validate the application of ISO 281 framework to predict the lifetime of main bearing of wind turbines, one would first have to filter out the failure cases caused by the trivial malfunctions outlined above. Once that is done, then, one could compare the failure rate of Figure 5.37 and Figure 5.38 with the observed failure rate of the Teesside wind farm. This has been done in Figure 6.1 where the failure rate based on both the basic L_n and the modified L_n predicted main bearing lifetime is compared with the

rolling failure rate of main drive train components of the Teeside offshore wind farm as recently reported by Moros et. al. Moros et al. (2024) and also described in Hiperwind deliverable report D5.3 Abrahamsen et al. (2024).

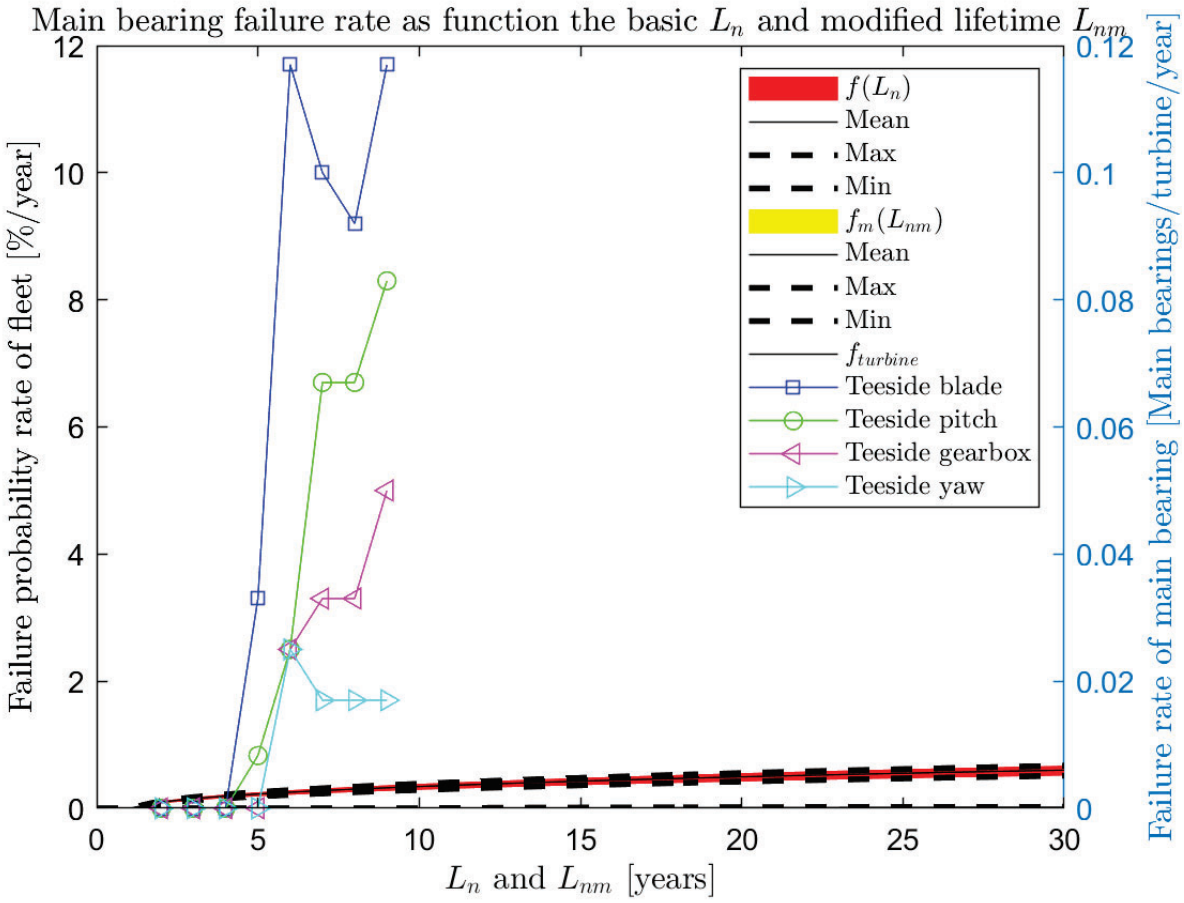

Figure 6.1: Failure rate of the main bearing of the Teesside turbines as function of the basic L_{ny} and modified L_{nmy} lifetime. The main bearing failure rate per year is compared to the rolling failure rates of the Teesside wind farm for the major drive train components as reported by Moros et. al. Moros et al. (2024).

It is observed that the predicted main bearing failure rate based on the basic L_n lifetime is about an order of magnitude lower than the observed failure rates of other components of the Teesside offshore wind farm in the first 9 years of operation. Secondly, the main bearing failure rate based on the modified lifetime L_{nm} is about two orders of magnitude below the previous Teesside drive train failure rates. Seen from the asset manager's point of view then, this result is very good because it confirms that the main bearing of the SWT 2.3 - 93 turbine is expected to be almost indestructible in the case of the Teesside wind farm. This is however posing a challenge in terms of validating the physics-based lifetime model of the main bearing, because the number of main bearing failures will be very small and might never show up for the Teesside wind farm. Thus a better approach for validation will probably be to include more wind farms and apply the methodology outlined in this report on all the SWT 2.3 - 93 offshore turbines installed and compare it with the combined failure statistics of the wind farms. This approach has not been attempted, but it is suggested to open discussions with organizations owning such data to

determine if it would be a possibility.

The question raised in the paper by Kenworthy et. al. "if the ISO 281 combined with the IEC 61400-1 standard is capable of predicting the lifetime of main bearing of wind turbines" was answered with a "probably not" by Kenworthy et. al. in the case of 1.5 MW GE onshore turbines. In the Hiperwind study of the Teeside wind farm, it does seem that the physics-based main bearing lifetime model is still in accordance with the observation that no main bearing failures are expected for the first 9 years of operation and that we do not expect to see many main bearing failures to appear. The main difference between the onshore case considered by Kenworthy et. al. Kenworthy et al. (2024) and the offshore case of Teesside might be the presence of de-humidifier systems keeping the temperature of the nacelle above 20 ^oC and also the humidity low in the Teesside turbines. The Hiperwind main bearing model did predict the temperature range of the main bearing (see Figure 5.10) and it matched the measured main bearing temperatures (see Hiperwind deliverable D5.3 Abrahamsen et al. (2024)) of the Teesside wind farm by assuming that main bearing temperature was always kept above 20 ^oC. This provides confidence that some of the ISO 281 framework ISO281 (2007) and TR1281-2 (2009) combined with the frictional torque description of Schaeffler in TPI 176 Schaeffler (2013) can replicate the main bearing heating (see Hiperwind deliverable D5.3 Abrahamsen et al. (2024)) and thereby also the expected change of the grease kinematic viscosity at different wind speeds and turbulence intensities (see Figure 5.11) and provide an indication of the viscosity ratio κ for the turbine operation points (see Figure 5.12).

The challenge of applying ISO 281 to the wind application might be connected to the determination of the lifetime modification factor a_{iso} from the previous operational parameters of the main bearing, since one will need to make assumptions on the grease cleanliness in terms of the e_C factor and combine this with the bearing load and the viscosity ratio. From Figure 5.13 and Figure 5.14 showing the resulting a_{iso} factor, it is seen that this is not a constant for all operation states of the turbine, and this will have a large impact on the resulting lifetime that is estimated. So even though the Hiperwind physics-based main bearing lifetime model is now capable of showing the influence of the turbine wind environment, it seems that the largest uncertainty remaining is how to include the effect of the a_{iso} factor and how to include the time changes of this. It has not been possible to establish how to evaluate the cleanliness of the grease of the Teesside offshore wind turbines and how to translate a measured $e_{C,measured}$ into a representative $e_{C,iso281}$ for the main bearing lifetime model. One way forward could be a campaign of collecting grease samples at a more regular interval than just the scheduled maintenance intervals and have these analyzed at a laboratory. A different approach could be to use the current physics-based model to obtain an estimate of e_C from the temperature variation of the main bearing and use that as an online condition monitoring-based estimate of e_C. A validation of such an approach could be performed by comparison to the SCADA data time evolution of a failing main bearing if that becomes available at the Teesside wind farm.

An interesting observation from the initial work of D5.1 was that it seemed that the aeroelastic simulation indicated that "the main bearing lifetime increased as the turbulence of the wind hitting the turbine was increased". The effect is clearly seen in both Figure 5.16 and Figure 5.17 for wind speeds around the rated wind speed of the turbine and when increasing either the turbulence intensity TI or the reference turbulence intensity I_{ref}. The effect is caused by the peak character of the turbine thrust curve around the rated wind speed, where the thrust force increases as wind speed raised to the power of 2 up until the rated wind speed. For higher wind speeds, the thrust force is decreasing because the pitch controller is starting to increase the pitch angle of the

blades. Since the main bearing loads are mainly a replica of the turbine thrust curve, then, the main bearing life is also shortest when the thrust force on the rotor is the highest according to the ISO 281 model. Thus increasing the turbulence around the rated wind speed will effectively distribute the thrust force away from the peak value of the thrust curve, and thereby result in a longer main bearing lifetime. This effect was not reported by Kenworthy et. al. Kenworthy et al. (2024), where they investigated if the IEC 61400-1 standard combined with the ISO 281 standard could be used to predict the lifetime of main bearings in a 1.5 MW GE turbine. They categorized the wind distribution into a low, a medium and high turbulence for the same annual average wind speed of 10 m/s of the Weibull distribution and focused on the wind shear as the main wind parameter to change. A decrease of the main bearing life from 142 years to 141 and 139 years is reported for low, medium and high turbulence respectively of a 240/630 bearing in a 1.5 MW GE onshore wind turbine with a shear of 0.2. No change with turbulence was observed for a 230/600 main bearing. It is believed that the relatively low number of 330 aeroelastic simulations in the Kenworthy study compared to the 33948 simulations of this study is the reason that the turbulence effect was not observed in the study of Kenworthy.

Finally, one can raise the question if physics-based main bearing lifetime models formulated from the ISO 281 and the IEC 61400-1 standards will have limitations in the future. One major challenge will be the growing diameter size of modern turbine main bearings, because many of the ISO 281 input parameters are not openly provided by the bearing manufacturers once the diameter is above 2 meters. This limit can be interpreted as the size in which the wind industry might be the major or only user of such bearings, whereby intellectual rights might be protected. However, a more general challenge is to determine the bearing rating parameters from experiments when the bearing diameter is above 2 meters because it will be quite expensive to test enough large bearings to obtain the properties purely based on experiments. Thus a possible application of the physics-based main bearing life models can be to determine the main bearing parameters from the turbine fleets as they start operating and thereby validate the model. Once the model is validated for a certain bearing sizes, then it might be used for new design of slightly larger main bearings. This application will only be possible for operators and OEM's with sufficient access to the turbine data and measurements.

7 Conclusions

A physics-based main bearing lifetime model has been formulated for the FAG 230/ 800 main bearing installed in the SWT 2.3 - 93 turbines of the Teesside offshore wind farm in the UK. The models is based on the standard ISO 281 "Roller bearings - Dynamic load ratings and rating life" and the IEC 61400-1 standard "Wind energy generation systems – Part 1: Design requirements". The IEC 61400-1 is used to compute the aeroelastic loads using the aeroelastic code Hawc2 of DTU and then the equivalent main bearing loads are evaluated using the ISO 281 framework.

The physics-based main bearing lifetime model is based on aeroelastic simulations of the SWT 2.3 - 93 turbines and the thrust force of the aeroelastic model has been validated against strain gauge measurement on one of the transition pieces on the offshore monopiles. The model has been used to provide a map of the expected main bearing basic lifetime L_{10y} of the wind turbines of the Teesside wind farm based on the measured average wind speed v_{ave} and reference turbulence intensity I_{ref} of each turbine. A basic L_{10y} life time between 24 and 29 years has been found as well as the failure probability of the Teesside wind farm. According to the basic

lifetime then the number of main bearings expected to fail is about 3 bearings in the 25 years of planned operation and with the first around year 12-15, the second around year 20-23 and the third around year 25-32.

A major attempt of the Hiperwind project has been to also include the life modification factor for system approach a_{iso} of the ISO 281 standard into account for the life time estimation, since this factor holds the potential of introducing the effect of operation condition of the main bearing into the life estimate. The main informations needed for estimating the life modification factor are the properties of the grease used to lubricate the bearing, the cleanliness of the grease during operation and finally the temperature of the bearing during operation. The physics-based model has been able to replicate the temperature operation range of the main bearings of the Teesside wind farm, whereby the uncertainty of the operating temperature has been reduced. Secondly, maps of the bearing grease properties and the bearing temperature have been obtained as functions of the turbine operation state in terms of the wind speed u and the turbulence intensity TI. These have been used to estimate the life modification factor a_{iso} for clean grease conditions of the Teesside turbines. The resulting modified main bearing lifetimes of the Teesside wind turbines are found to be between 210 and 290 years, which is so long that one would conclude that the main bearings are indestructible. This should, however, be seen as the upper limit of the main bearing life since a much shorter lifetime will result if the contamination factor e_C of the grease is taken into account or if the supporting system of re-greasing the bearing or the seals of the main bearing are degrading. It has not been possible to estimate the e_C value of the Teesside main bearings, but a conservative estimate of the main bearing lifetime, if operated properly, is in between the basic lifetime of 24-29 years and the modified lifetime of 210-290 years. This matches the observed failure statistics of the Teesside wind farm, where no main bearing failures have been observed after 9 years of operation. It will be interesting to follow the development of the Teeside main bearing failures to determine if the basic or the modified lifetime is replicating the behavior best. From the analysis of the Hiperwind project, it is clear that the formulation of time-dependent life modification factors and how to incorporate them into the simulations, as well as the equivalent loads estimations, remains the largest source of uncertainty of the validation of the physics-based main bearing life model. This work is suggested as a future challenge to the wind research community.

Acknowledgements

This work is a part of the HIghly advanced Probabilistic design and Enhanced Reliability methods for the high-value, cost-efficient offshore WIND (HIPERWIND) project, which has received funding from the European Union's Horizon 2020 Research and Innovation Programme under Grant Agreement No. 101006689. The support is greatly appreciated. The authors gratefully acknowledge the computational and data resources provided on the Sophia HPC Cluster at the Technical University of Denmark, DOI: 10.57940/FAFC-6M81 .

References

A. B. Abrahamsen, S. Dou, A. Zeghidour, N. Berranah, and C. Jacquet. Hiperwind deliverable report d5.3 - physics-based component model validation. Technical report, H2020 HIPERWIND project (Grant agreement No 101006689), 2024.

S. Bannister and R. McCall. Offshore decommissioning plan: Teesside offshore windfarm. Technical report, PPMS, 2011.

R. G. Budynas and J. K. Nisbett. *Shigley's mechanical engineering design*. McGraw-Hill series in mechanical engineering. McGraw-Hill, 9th ed edition, 2011. ISBN 978-0-07-352928-8.

IEC61400. Iec 61400-1:2019 wind energy generation systems – part 1: Design requirements. Technical report, IEC, 2019.

ISO281. Rolling bearings – Dynamic load ratings and rating life: DS/ISO 281:2007. Technical report, ISO, 2007.

J. Kenworthy, E. Hart, J. Stirling, A. Stock, J. Keller, Y. Guo, J. Brasseur, and R. Evans. Wind turbine main bearing rating lives as determined by iec 61400-1 and iso 281: A critical review and exploratory case study. *Wind Energy*, 27(2):179–197, 2024. doi: https://doi.org/10.1002/we.2883. URL https://onlinelibrary.wiley.com/doi/abs/10.1002/we.2883.

T. J. Larsen and A. M. Hansen. How 2 hawc2, the user's manual. Risø-R-1597(ver. 13.0)(EN) 0 ISBN 978-87-550-3583-6, DTU Wind and Energy Systems, 2023.

D. Moros, N. Berrabah, K. D. Searle, and I. G. Ashton. Maintenance & failure data analysis of an offshore wind farm. *Journal of Physics: Conference Series*, 2767(6):062006, jun 2024. doi: 10.1088/1742-6596/2767/6/062006. URL https://dx.doi.org/10.1088/1742-6596/2767/6/062006.

A. K. Papatzimos, T. Dawood, and P. R. Thies. Data insights from an offshore wind turbine gearbox replacement. *Journal of Physics: Conference Series*, 1104(1):012003, oct 2018. doi: 10.1088/1742-6596/1104/1/012003. URL https://dx.doi.org/10.1088/1742-6596/1104/1/012003.

B. Paz, L. Yi-chao, N. Marx Hermoso, W. Remigius, and A. B. Abrahamsen. Hiperwind deliverable report d5.2 - electrical grid model. Technical report, H2020 HIPERWIND project (Grant agreement No 101006689), 2023.

D. Remigius, B. Paz, Y. Liu, W. Remigius, and A. B. Abrahamsen. Hiperwind deliverable report d5.1 - component life models. Technical report, H2020 HIPERWIND project (Grant agreement No 101006689), 2023.

Schaeffler. Tpi 176 : Lubrication of rolling bearings. Technical report, "Schaeffler Technologies", 2013.

Siemens. Outstanding efficiency siemens wind turbine swt-2.3-93. order no. e50001-w310-a102-v6-4a00. Technical report, Siemens, 2009.

TR1281-2. Rolling bearings – Explanatory notes on ISO 281 – Part 2: Modified rating life calculation, based on a systems approach to fatigue stresses : DS/ISO/TR 1281-2:2008(e). Technical report, ISO, 2008.

TR1281-2. Rolling bearings – Explanatory notes on ISO 281 – Part 2: Modified rating life calculation, based on a systems approach to fatigue stresses: DS/ISO/TR 1281-2:2009, 2009.